TMT4905 - Materials Technology, Master's Project

# Hydrogen permeation in different microstructures of 66SiMnCrMo6-6-4 steel

**Christian Vågenes**

Supervisor: Andreas Erbe

In cooperation with Kverneland Group

Spring 2023

# Preface

This master thesis has been written in cooperation with SINTEF and the Kverneland Group at the Norwegian University of Science and Technology, under the master course TMT4905. Despite the hardships and challenges which I have had to go through while doing my experiments and writing this thesis, I have still been able to obtain interesting results - and finally begun to master using the Devanathan-Stachurski cell. Although I was not able to finish everything I wanted to do, like TDS and the D samples, I still believe that the results found in this thesis are fruitful and provide a proper contribution to the total of human knowledge. I want to thank Andreas Erbe once again for being my supervisor throughout the entire thesis and his help. I would also like to thank Erlend Sølvberg for his inputs, and I hope he finds the results as useful as I did. Another special thank you to Erik Aas Koren and Iman Taji, who both have helped out and made suggestions and contributions that have had significant impact on this thesis. And finally, I would like to thank my father Geir Vågenes, my mother Rie Bønsøe and my girlfriend Chloe Corner, who have all been there to support me throughout my academic journey all the way to where it is today.

# Abstract

The diffusivity of hydrogen in steel is dictated by various mechanisms which causes brittleness. Depending on the microstructure, hydrogen embrittlement can be caused by a plethora of mechanisms, which therefore makes it challenging to accurately predict the behaviour of hydrogen introduced to the bulk material. Diffusion experiments of B240, B280, QT440 and Q microstructures of the 66SiMnCrMo6-6-4 steel were performed, and each sample was tested three times to produce three different transients. These transients were then compared and steady-state normalized to research the trapping abilities of all microstructures. The results which were obtained showed that QT440 had a slightly higher hydrogen diffusivity and steady state flux than the other microstructures of the same steel, and its lower content of austenite is believed to be the reason. Compared to other steels the hydrogen permeability was still significantly lower than average, but by using the formula of Boellinghaus(Boellinghaus et al., Welding in the World, vol. 35, 1995, p. 149) it was found that the findings are still plausible, as the diffusion constant is higher than the minimum logical diffusion coefficient in steel. Irreversible and reversible trapping was looked into, and while there were little or no irreversible traps seen, all microstructures did show signs of reversible trapping. Therefore it is concluded that the alloy is generally very permeation resistant.

# Contents

# Acronyms

| | |
|---|---|
| **BCC** | Body-Centered Cubic |
| **BCT** | Body-Centered Tetragonal |
| **CE** | Counter Electrode |
| **FCC** | Face-Centered Cubic |
| **HE** | Hydrogen Embrittlement |
| **ISO** | International Organization for Standardization |
| **LOM** | Light Optical Microscopy |
| **RE** | Reference Electrode |
| **SCE** | Saturated Calomel Electrode |
| **SD** | Standard Deviation |
| **TDS** | Thermal Desorption Spectrometry |
| **UTS** | Ultimate Tensile Strength |
| **WE** | Working Electrode |

# List of Figures

# List of Tables

# 1 Introduction

The ever-increasing relevance of hydrogen embrittlement in the steel industry is underlining the necessity of research around the topic. Stronger steels are designed for many purposes, among those to increase wear resistance while simultaneously lower the weight of constructions and equipment. Hydrogen embrittlement in steels becomes a more and more significant factor the stronger the steel is, and as a rule of thumb, steels with an ultimate tensile strength exceeding 1000 MPa[1, 2] are at risk of becoming severely weakened by this phenomena. Several mechanisms contributing to the detrimental effect of HE[3].

This master thesis seeks to provide more information on the 66SiMnCrMo6-6-4 alloy - a steel mainly used in heavy industry bearings - by investigating the hydrogen permeation through different microstructures. The composition of the alloy is detailed in the table below - a medium carbon steel with a high silicon and manganese content. A full list of its contents is detailed in table 1.1. By heat treating the steel in different ways, several microstructures arise. All four microstructures, which are explained in further detail under the 3.1 section, were permeation tested, and a look into irreversible and reversible trapping was performed. The implications of the results have been further discussed in this thesis, and the roles of martensite, bainite, residual austenite and cementite have been investigated.

A Devanathan-Stachurski permeation cell was used for this experiment, in which the steel samples act as a membrane in which hydrogen diffuses through. Light-optical microscopy images were taken to look into the compositions of each microstructure, and hardness tests were also taken, to ensure that the hardness is sufficient for hydrogen embrittlement to be relevant.

| Steel | C % | Si % | Mn % | P % | S % | Cr % | Ni % | Mo % | Cu % |
|---|---|---|---|---|---|---|---|---|---|
| 66SiMnCrMo6-6-4 | 0.65 | 1.5 | 1.37 | 0.016 | 0.001 | 1.01 | 0.12 | 0.23 | 0.126 |

**Table 1.1:** *The content of the 66SiMnCrMo6-6-4 steel used in the experiments. The steel was produced by Ovako AB, then heat treated by Kverneland.*

# 2 Theory

## 2.1 On steel matrices and hydrogen diffusion

Diffusion of hydrogen occurs when atomic hydrogen is present. The most relevant method of diffusion for this thesis happens when hydrogen is adsorbed onto the surface of the metal, bonding with an electron, and then further absorbed into the metal, as shown by equation 2.1 and 2.2[4, 5]:

$$H^+ + e^- \longrightarrow H_{adsorbed} \tag{2.1}$$

$$H\_adsorbed \longrightarrow H_{absorbed} \tag{2.2}$$

Diffusivity rates of hydrogen vary depending on the phase of material, although most relevant in this thesis would be martensite, austenite and ferrite – three common phases found in steel. Martensite in particular is the most relevant for HE, as the diffusion in these structures is higher than in ferrite[4, 6]. Defect lattices enable hydrogen accumulation to a larger extent, as shown by the works of Luo and Song[7, 8], which to some extent explains why BCT is prone to HE. Ferrite is more susceptible to hydrogen embrittlement than austenitic steel[4], but ferrite has a low tensile strength. Steels with austenitic and martensitic phases, however, have properties which ferritic steels cannot match – and therefore exhibits a greater tensile strength than any ferritic steel is capable of. Given that hydrogen is attracted to stress crack tips[6, 9], the driving force of embrittlement becomes larger as the load on the specimen increases. However, HE is caused by several mechanisms and is therefore impossible to attribute to a single property of a metal[10]. HE is dependent on both environmental and material factors. Internal pressure from hydrogen recombining inside of the metal, the formation of metal hydrides (manganese hydride, to provide an example from this thesis) and even inducing phase transformations within steel are some of the mechanisms which have been discussed to happen within steel[11–13]. HE is only relevant for steels with an UTS greater than 1000 MPa[10], and in environments with high prevalence of hydrogen – seawater and high moisture climates are therefore a threat to high-strength steel alloys[10, 14, 15]. Depending on the alloy and microstructure[16], certain steels may have hydrogen traps inside of them. A trap will immobilize hydrogen before it is allowed to react with the bulk steel, and

traps can be introduced by adding certain microstructural constituents or elements[17, 18]. Traps can be either reversible or irreversible, depending on the trapping energy. At ambient temperatures, a trap is considered irreversible if the trapping energy is above 50-60 kJ/mol. Increasing the temperature will release most trapped hydrogen.[4] Irreversible traps are determined by comparing the first transient to the second and third transient - if the consecutive transients begin sooner than the first transient, irreversible trapping is occuring. Reversible trapping is determined by comparing the transients to Fick's ideal curve - if the transients are steeper than the ideal curve, reversible trapping is occurring[19, 20]. A major challenge with diffusion experiments is reflected in the time it takes to diffuse through a sample. For certain alloys, a steady state diffusion is reached after a very long time – experiments can last up to 2-4 weeks for a 100µm thick sample![4]. Therefore, certain methods are used to accelerate the diffusion time of certain samples. Producing very thin samples is one way of reducing diffusion times, and increasing the temperature will also lead to faster diffusion.[4] A third way of accelerating the process is accomplished by adding a hydrogen recombination poison – which inhibits the ability of adsorbed hydrogen to recombine into $H_2$, thus reducing the rate of which adsorbed hydrogen can recombine and become hydrogen gas. The poison used in this thesis is thiourea, however, cyanides, arsenic, and antimony, among others, can also slow down the hydrogen gas production[21]. A Pd coat was deemed necessary to add, seeing as it is necessary for good experimental data, according to several sources[22–24].

## 2.2 Permeation transients

A permeation transient contains information about the diffusion coefficient within the alloy. By working through different formulas, which will be explained in detail, with the parameters found in the permeation experiments, an attempt on finding the diffusivity coefficient for each steel is made. First off, the sub-surface concentration of hydrogen at the cathodic side of the sample is determined by using formula 2.3 and 2.4:

$$J_{SS} = \frac{I_{SS}}{AF} \tag{2.3}$$

$$J_{SS} = \frac{D_l C_0}{L} \tag{2.4}$$

Where $J_{ss}$ constitutes the steady state hydrogen permeation flux which occurs on the anodic side, $I_{ss}$ is the steady state current, $A$ is the area of exposure, $L$ is the sample thickness and $F$ is Faraday's constant. $C_0$ denotes the sub-surface concentration of hydrogen atoms in interstitial lattice sites on the cathodic side, while $D_l$ describes the lattice diffusion coefficient. $D_l$ is temperature-dependent and therefore exhibits typical Arrhenius behaviour:

$$D_l = D_0 \cdot \exp(\frac{-E_l}{RT}) \tag{2.5}$$

With $T$ naturally describing temperature and $R$ being the gas constant; $E_l$ is the interstitial lattice site jump activation energy, and $D_0$ is the frequency factor. For the case of pure BCC iron, $E_l$ is $5.69x10^3 Jmol^{-1}$ and $D_0$ is $7.23x10^{-8} m^2 s^{-1}$. These values are valid for temperature ranges between -40°C and +80°C[25]. For certain situations, the diffusion matrix will vary to a large extent between different phases – multiphase steels and highly alloyed metals are good examples of this. For such scenarios another formula for $J_{ss}$ can be considered:

$$J_{SS} = \frac{D_{eff} C_{0R}}{L} \tag{2.6}$$

With $D_{eff}$ denoting the effective diffusion coefficient, and $C_{0R}$ being the sum of all hydrogen in interstital lattice sites as well as in reversible traps. This is of relevance as the steel has a multiphase structure, as detailed by ISO 17081, however, it was decided to only use equation 2.3 and 2.4 for this thesis as $C_{0R}$ requires the amount of reversible traps to be known, which would require further experimentation.

Furthermore, $D_{eff}$ can be found by using the formulas 2.7 and 2.8:

$$D_{eff} = \frac{L^2}{6t_{lag}} \tag{2.7}$$

$$D_{eff} = \frac{L^2}{15.3t_b} \tag{2.8}$$

In this thesis only the $t_{lag}$ method is used, with $t_{lag}$ denoting the time it takes for $J(t)/J_{ss}$ to reach 0.63. The validity of the $t_{lag}$ method described in formula 2.7 is disputable for situations where low alloy steels are used[26], however, according to ISO 17081 both formulas are valid[19]. Each formula is explained further in depth in ISO 17081 and ASTM G148-97[20], with an exception of formula 2.5.

# 3 Experimental

## 3.1 Steels

In this thesis 4 microstructures were tested. The steel, 66SiMnCrMo6-6-4, has been put through different heat treatments, and a closer look at the microstructures is necessary to provide context to the results.

The different samples all have the same composition, with various heat treatment cycles. The treatments are described in detail here:

**As-delivered (D)**

No heat treatment has been performed after delivery from the supplier. The steel therefore has a ferritic microstructure, complimented by spherodized cementite. NOTE: D was dropped from the experiments, yet remain in the thesis as a point of comparison to the heat treated steels.

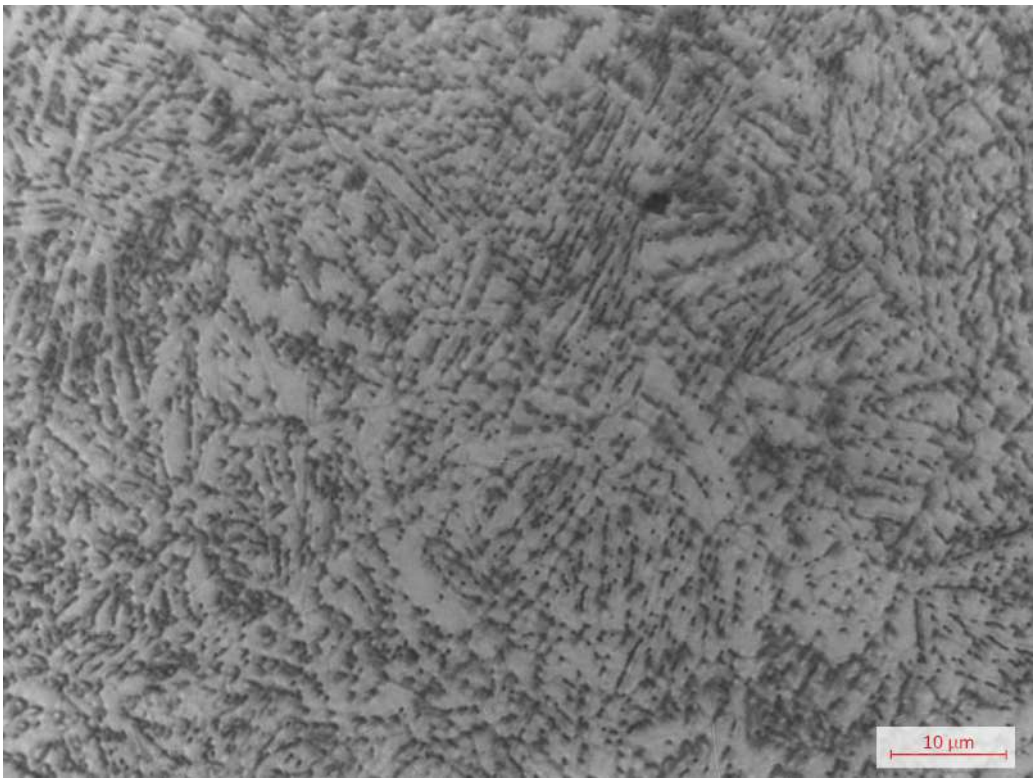


**Figure 3.1:** *Microstructure of D, with a ferritic matrix containing spherodized cementite. 1000x magnification.*

**Quenched (Q)**

This microstructure arises when the steel is initially heated to 930°C and kept at this temperature for 40 minutes. The steel is then quenched in a salt bath maintaining 180°C – water is not used to avoid quench cracks from internal strain. Finally, the steel is allowed to air cool until room temperature is reached. The microstructure produced is martensitic with residual austenite.

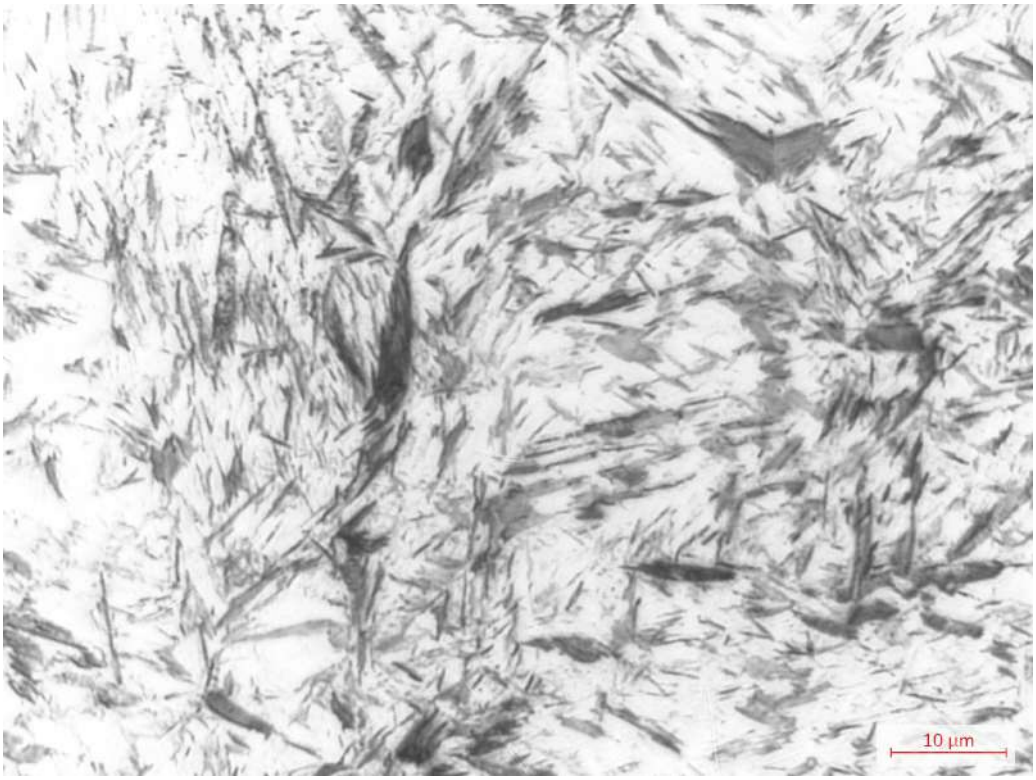


**Figure 3.2:** *Microstructure of Q, containing quenched martensite with residual austenite. 1000x magnification.*

**Isothermally transformed (B240)**

Like the Q steel, this steel is also heated to 930°C. Once the heating procedure is completed, the steel is quenched in a salt bath to 240°C, then held at this temperature in an oven for 15 hours before the steel is allowed to air cool to room temperature. This produces a structure from the lower regions of bainitic steel.

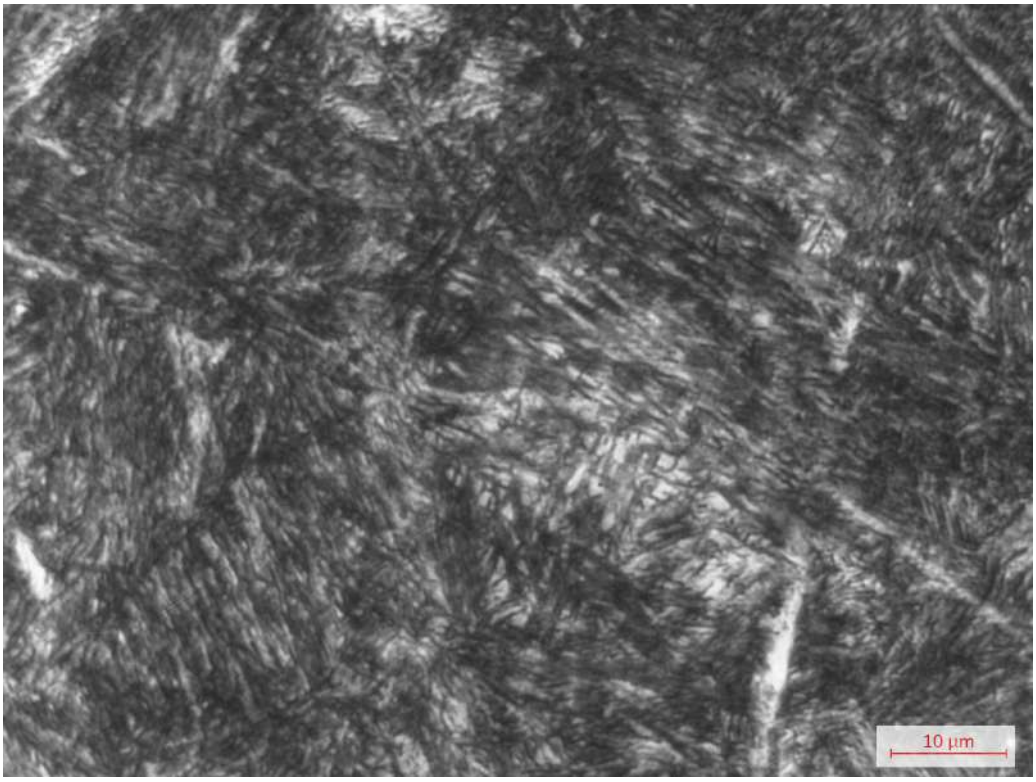


**Figure 3.3:** *Microstructure of B240, displaying a bainitic steel including retained austenite. 1000x magnification*

**Isothermally transformed (B280)**

Exactly like the B240 steel, except for the fact that the salt bath is holding 280°C. A slightly coarser bainitic structure is produced.

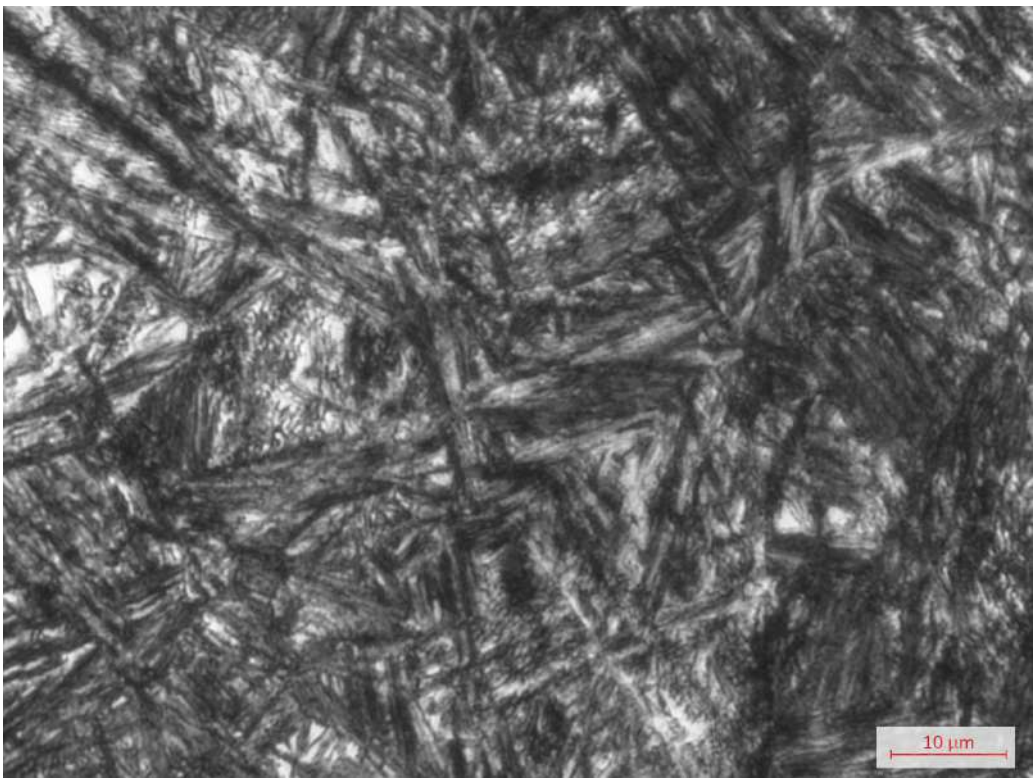


**Figure 3.4:** *Microstructure of B280, showing a slightly coarser bainitic steel with retained austenite. 1000x magnification.*

**Quenched and tempered (QT440)**

The tempered steel is treated like the Q steel but tempered at 440°C for 2 hours after being cooled to room temperature. This process is then repeated to further temper the newly generated martensite.

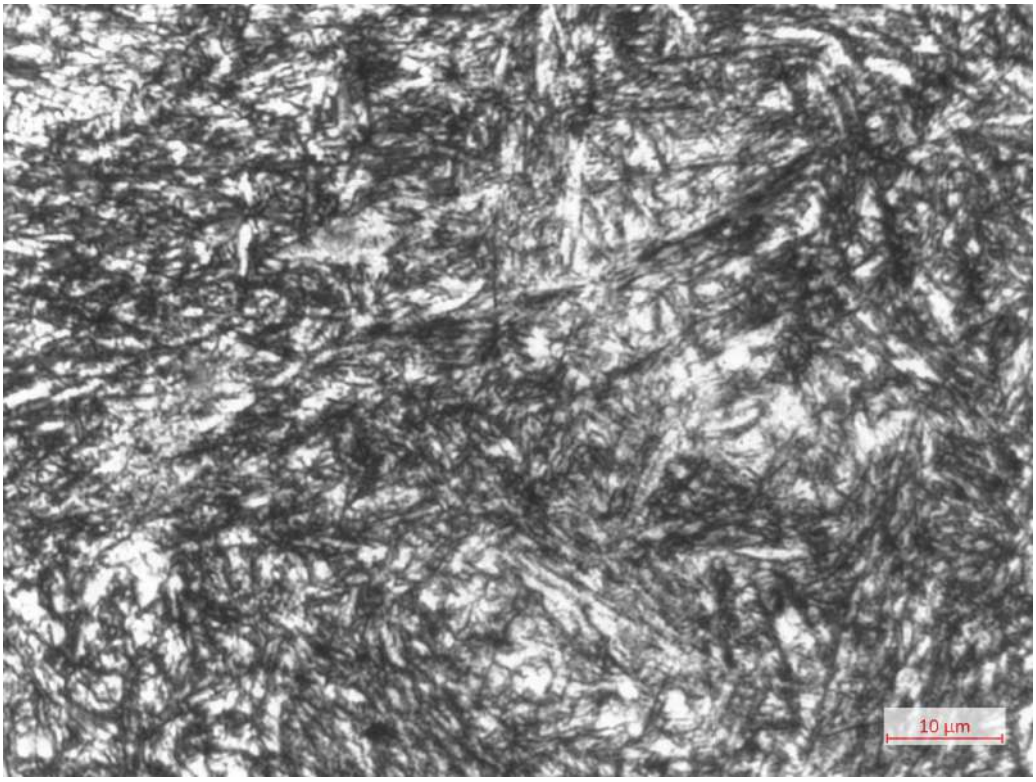


**Figure 3.5:** *Microstructure of QT440, containing tempered martensite, retained austenite as well as carbides. 1000x magnification.*

## 3.2 Sample preparation

### 3.2.1 Characterization and hardness testing of samples

All microstructures were polished, etched in 2% nital and then photographed at 1000 times magnification with a standard Zeiss light-optical microscope. The samples used for LOM were not part of the experiment. Black and white photographs were utilized for the sole reason that these images were more clear than their coloured counterparts. A hardness test was also conducted with an Innovatest hardness machine – 5 well spaced indents were made for each microstructure and the average Vickers hardness was found.

### 3.2.2 Machining & surface preparation

A sample of each microstructure was cut into slices of approximately 1 mm, and the surface was ground down with SiC-paper, starting at P320 and then progressively working towards a P4000 finish. The sample thickness was then checked – this was performed in 5 different spots, and the average thickness was then recorded. Any sample with a greater thickness deviation than 5% were discarded, as per ISO 17081[19] standards. The sample was then cleaned in a sealed container filled with acetone in an ultrasonic bath for 5 minutes to remove any contaminations from the surface.

### 3.2.3 Pd coating

A solution of approximately 0.35 mM Pd-complex was made by adding 7 mL $Na_2[Pd(NO_2)_4]$ to $0.1M$ NaOH, which acted as the electrolyte. The same diffusion cell utilized for the experiment itself was used to deposit a layer of palladium onto the sample by using a three-electrode setup. The sample itself was used as the working electrode, an inert platinum rod with a greater surface area than the sample itself as a counter electrode, and an SCE as the reference electrode. A Gamry Reference 600 potentiostat was used to apply a galvanostatic current of $-100$ µA/cm$^2$, and the solution was deoxygenated by bubbling nitrogen through the solution for 5 minutes before adding the Pd salt. The coating process was then run for another 55 minutes, totalling 1 hour per sample. The samples were then transferred to an oven holding 110°C and degassed for 10-20 hours, which depleted any unwanted trapped hydrogen introduced during the coating process. Each sample was degassed at 110°C in a furnace for 10-20 hours before any experiment

was done, as well as the chamber itself, gaskets, and the sample holder.

**Figure 3.6:** *The Pd coating made a visible deposit on the samples.*

### 3.2.4 Diffusion cell setup and experiments

The diffusion cell setup is a Devanathan-Stachurski cell, as seen in figure 3.7. This cell is set up with two three-electrode cells sandwiching the two sides of a shared working electrode – the sample itself. An inert platinum counter electrode was used, and an SCE as reference electrode for the anodic side. The cathodic side used an Ag/AgCl electrode. Nitrogen was bubbled through the electrolyte on both sides to purge the oxygen from the solution, preventing surface disturbances and corrosion on the sample. The anodic side was set to run potentiostatically; a +300 mV vs. SCE potential was applied. The cathodic side was run galvanostatically with a -1 mA/cm$^2$ current. Both chambers used a 0.1 M NaOH electrolyte, and thiourea was added to the charging chamber (with an exception of B240 sample 1 and 2, transient 1), at 2 g/L of electrolyte. The values and electrolyte used here are originally derived from the thesis written by Husby[27] and ISO 17081[19], and modified to suit this experiment, as explained in further detail under section 5. Three samples of each microstructure were made, and each sample was run 3 times to investigate reversible traps for the microstructures. All samples had a diameter of approximately 23 mm, but with the gaskets applied on both sides of the sample the exposed diameter was only 14.95 mm. In total, the exposed area on one side therefore become 1.754 cm$^2$ for all samples. The charging started when steady state was obtained, usually after 20000-30000

seconds. Each experiment was halted after 20-30 hours of total runtime, at which point steady-state was obtained. Every sample was run 3 times to produce 3 transients – with at least 24 hours of resting time in a desiccator between each run. A different cell design was used for QT440 and Q samples, without the teflon fitting as seen in figure 3.8.

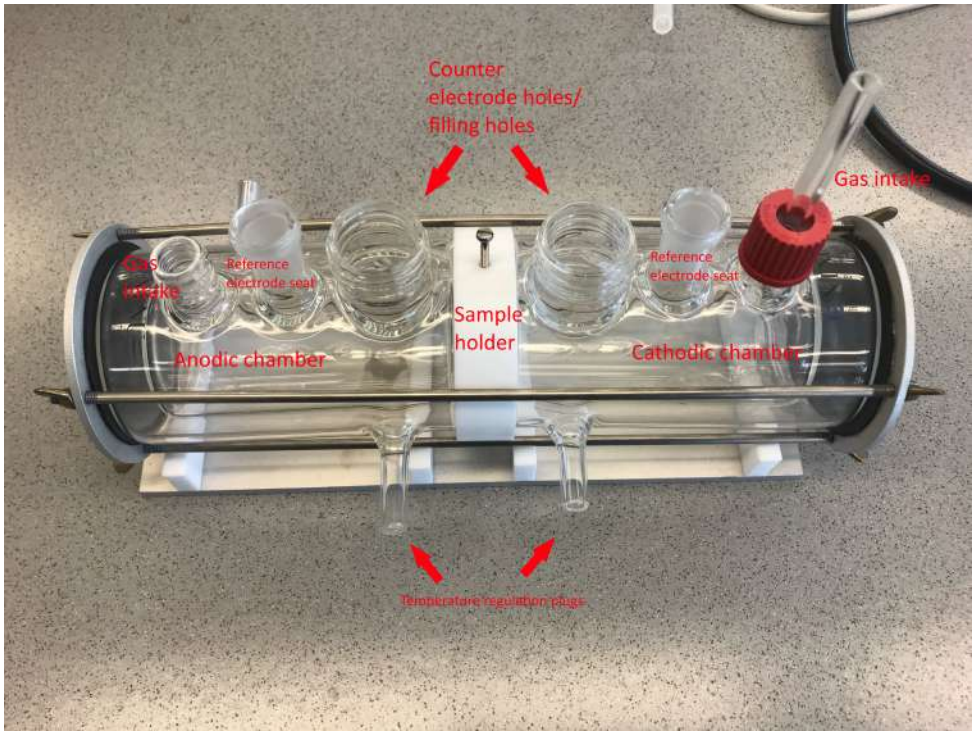


**Figure 3.7:** *The diffusion cell setup with its components labelled. The temperature regulation plugs allow temperature control by sending water at a given temperature through, which heats the chamber inside without making contact with the water. This was not used in this experiment.*

**Figure 3.8:** *The teflon fitting which was prone to leakages during the B240 and B280 experiments. It was positioned between the sample holder and the cell chambers, see figure 3.7.*

# 4 Results

## 4.1 Hardness tests

A hardness test was conducted for all samples, with 5 separate, well spaced indents per microstructure. The average of all indents were measured.

| Microstructure | Average ± SD |
|---|---|
| D (HV) | 229.1 ± 3 |
| Q (HV) | 857.5 ± 15 |
| B240 (HV) | 662.1 ± 6 |
| B280 (HV) | 589.7 ± 9 |
| QT440 (HV) | 555.9 ± 8 |

**Table 4.1:** *Average hardness results for all microstructures. Parameters used in test are stated above. A 5kg force was applied for D, 10kg for the other samples. Holding time 15 seconds.*

## 4.2 Sample thickness

As explained in the former section, each sample had to have a variation in thickness of less than 5%. Each sample had its thickness measured in 5 spots as shown in the figure below. Table 4.2 shows the average thickness of each sample, as well as the greatest deviation

from average.

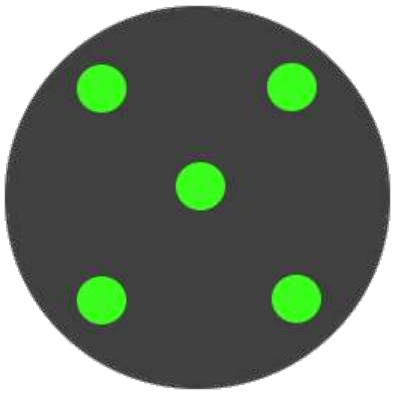

**Figure 4.1:** *Each dot represents where a thickness measurement was performed on each sample.*

| Microstructure | Average | Max. deviation | Microstructure | Average | Max. deviation |
|---|---|---|---|---|---|
| B240 1 | 1.04mm | 3% | QT440 1 | 1.05mm | 3% |
| B240 2 | 0.863mm | 1% | QT440 2 | 1.21mm | 2% |
| B240 3 | 0.903mm | 1% | QT440 3 | 1.02mm | 1% |
| B280 1 | 1.08mm | 1% | Q 1 | 1.49mm | 2% |
| B280 2 | 0.790mm | 2% | Q 2 | 1.22mm | 2% |
| B280 3 | 1.01mm | 1% | Q 3 | 1.19mm | 1% |

**Table 4.2:** *Listed average thickness and deviation for every produced sample which were tested.*

| Microstructure | $I_{ss}$ $[\mu A/cm^2]$ | $J_{ss}$ $[mol \cdot m^{-2} \cdot s^{-1}]$ | $t_{lag}$ $[s]$ | $D_{eff}$ $[cm^2 \cdot s^{-1}]$ |
|---|---|---|---|---|
| B240 1 | 150 | $8.20 * 10^{-8}$ | 18075 | $1.00 * 10^{-11}$ |
| B240 2 | 235 | $9.40 * 10^{-8}$ | 12575 | $1.44 * 10^{-11}$ |
| B240 3 | 270 | $8.39 * 10^{-8}$ | 11755 | $1.54 * 10^{-11}$ |
| B280 1 | 150 | $8.33 * 10^{-8}$ | 17215 | $1.13 * 10^{-11}$ |
| B280 2 | 195 | $8.62 * 10^{-8}$ | 19435 | $1.00 * 10^{-11}$ |
| B280 3 | 220 | $9.64 * 10^{-8}$ | 22575 | $8.63 * 10^{-12}$ |
| QT440 1 | 240 | $1.22 * 10^{-7}$ | 8710 | $2.10 * 10^{-11}$ |
| QT440 2 | 275 | $1.16 * 10^{-7}$ | 3005 | $6.07 * 10^{-11}$ |
| QT440 3 | 295 | $1.28 * 10^{-7}$ | 3840 | $4.75 * 10^{-11}$ |
| Q 1 | 153 | $5.57 * 10^{-8}$ | 15110 | $1.65 * 10^{-11}$ |
| Q 2 | 175 | $6.73 * 10^{-8}$ | 18405 | $1.35 * 10^{-11}$ |
| Q 3 | 156 | $6.86 * 10^{-8}$ | 22625 | $1.10 * 10^{-11}$ |

**Table 4.3:** *Parameters which were found for the successful runs included in the results part, with the 1, 2 and 3 denoting their respective transients (see appendix for further results).*

## 4.3 Permeation transients

The parameters of each transient are shown in table 4.3. Each curve has been cropped to start at the point where charging begins. Steady state current density for each curve is set to 0. The temperature in the room was measured to be 23°C after the experiments. The Fick curve in the normalized graphs denotes the ideal diffusion curve as described by Fick's 2nd law.

### 4.3.1 B240

The B240 transients were mostly defined by a sharp rise for each transient, indicating a rapid penetration. The permeation transient begins after about 5000 seconds, and stops after 30000-40000 seconds.

### 4.3.2 B280

The B280 microstructure has a significantly slower permeation compared to B240. Permeation starts at around 7500 seconds and does not stop before about 40000-50000 seconds, with the exception of sample 2, which resembles B240.

### 4.3.3 QT440

The QT440 samples had the quickest permeations of all microstructures. Variations in current density before steady state at around 30000 seconds were present with QT440 as well.

### 4.3.4 Q

The permeation curves of Q indicates very slow hydrogen permeation. The Q microstructures also had significantly lower steady state currents compared to the other samples. The curves did not have problems with irregular curves to the same extent, but there were some transient variation.

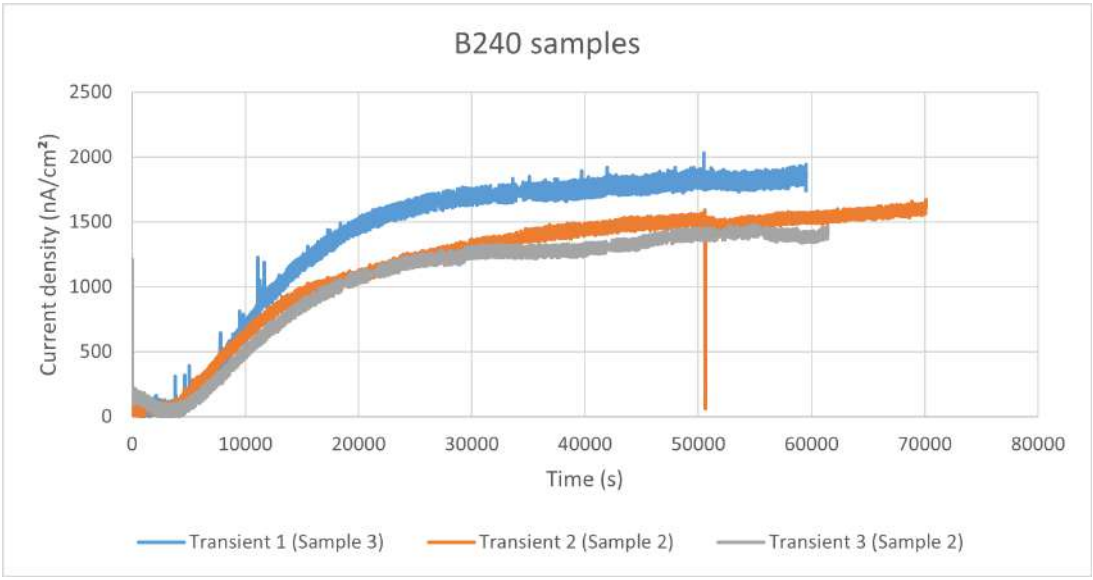


**Figure 4.2:** *The permeation transients for sample 3 (1st transient) and 2 (2nd and 3rd transient) B240.*

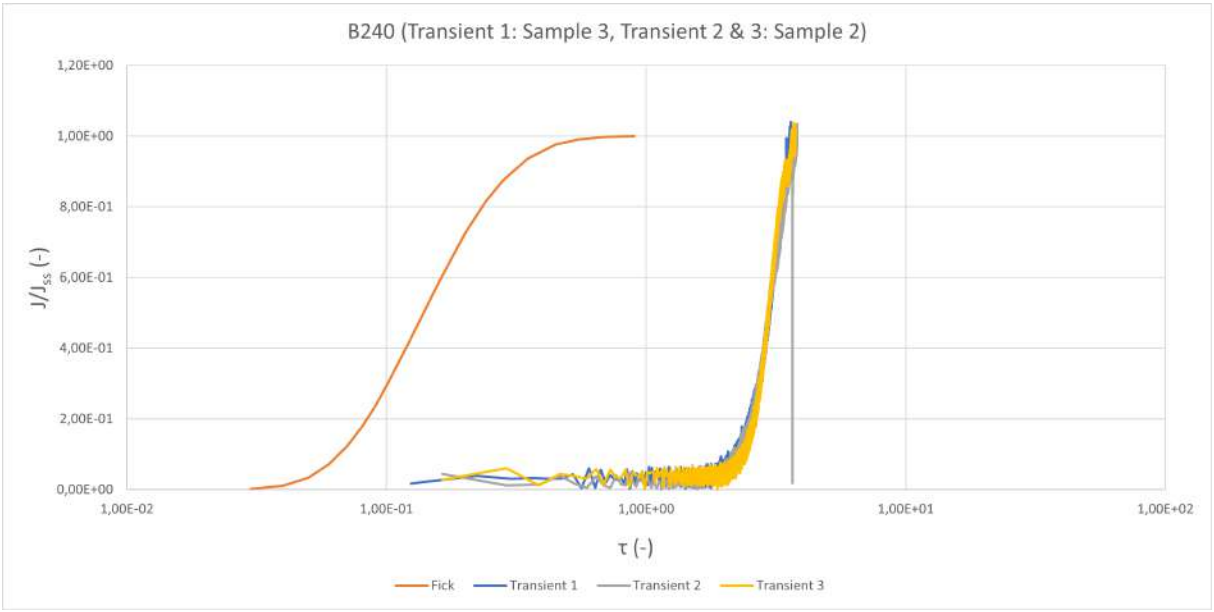


**Figure 4.3:** *The steady state permeation transients for sample 3 (1st transient) and 2 (2nd and 3rd transient) vs. normalized time.*

Further results have been included in the appendix.

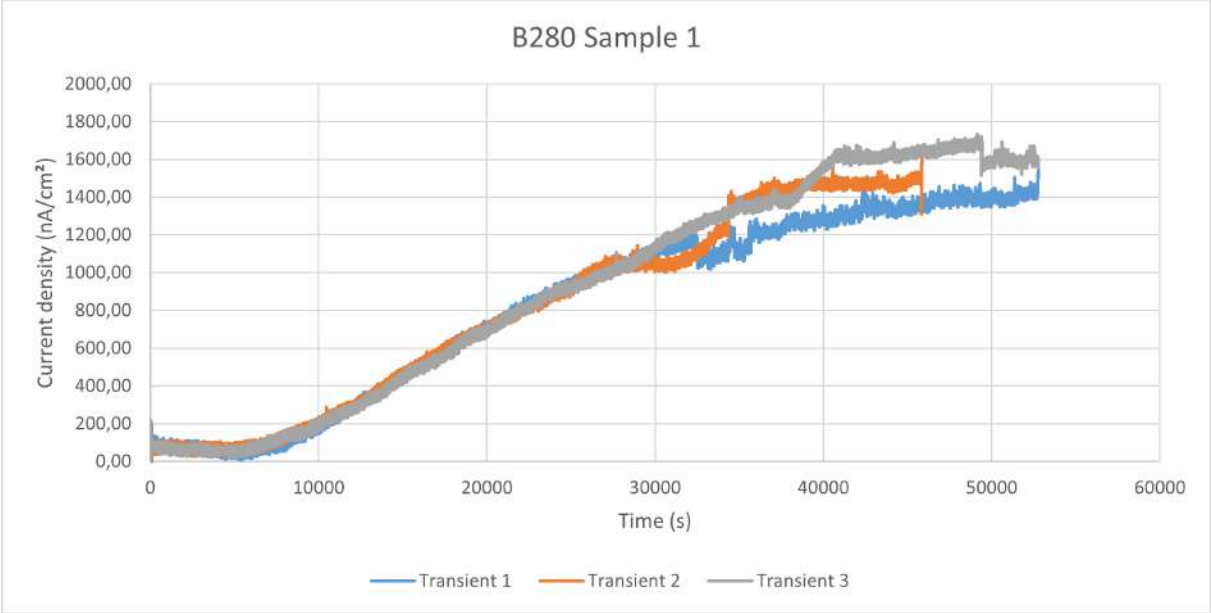


**Figure 4.4:** *The permeation transients for the 1st B280 sample.*

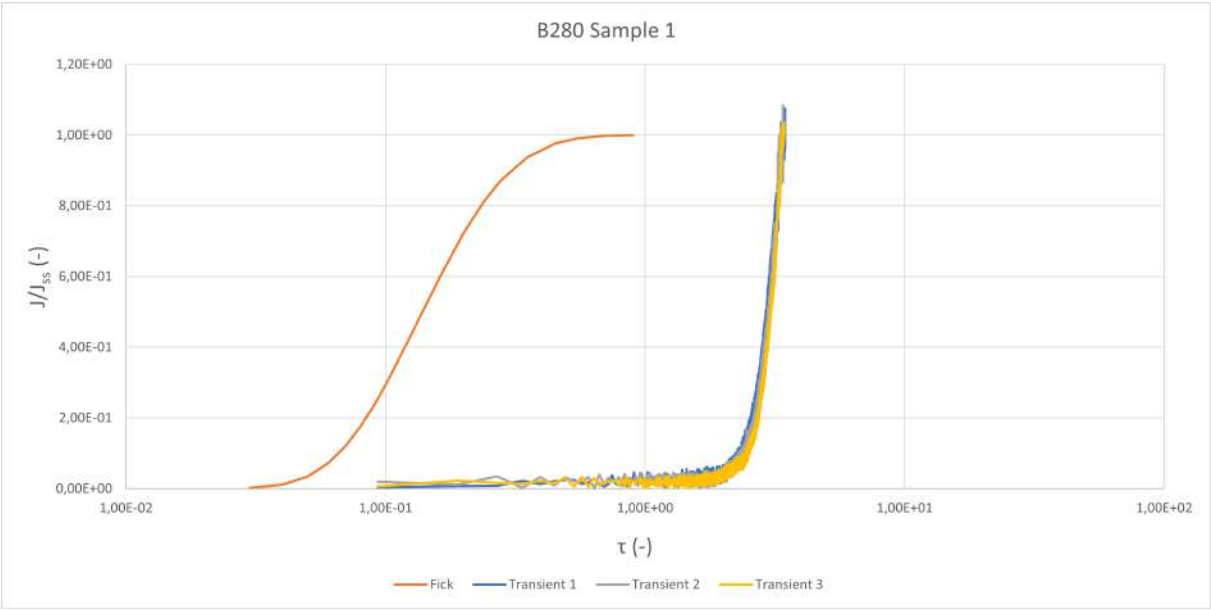


**Figure 4.5:** *The steady state permeation transients for the 1st B280 sample vs. normalized time.*

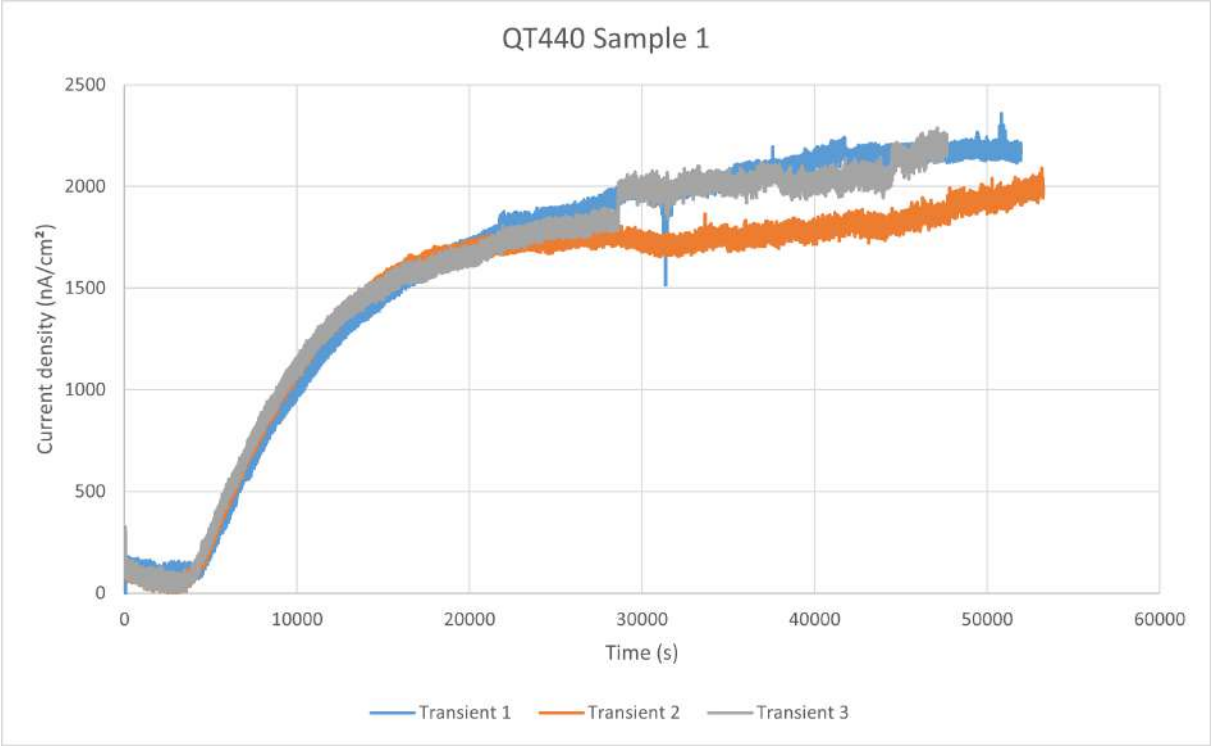


**Figure 4.6:** *The permeation transients for the 1st QT440 sample.*

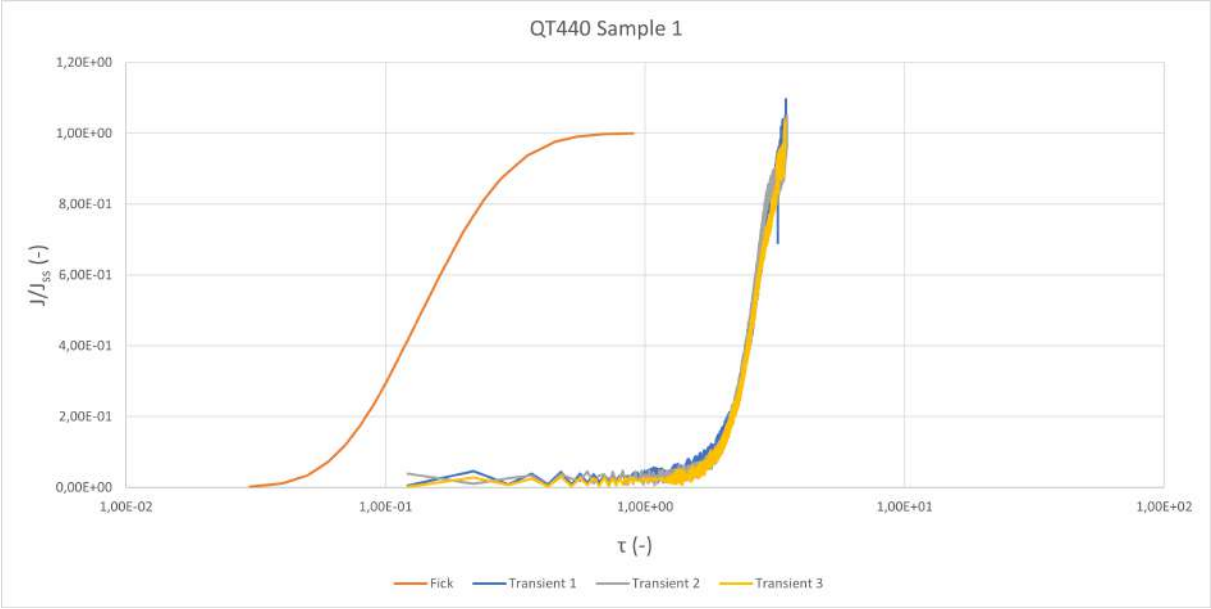


**Figure 4.7:** *The steady state permeation transients for the 1st QT440 sample vs. normalized time.*

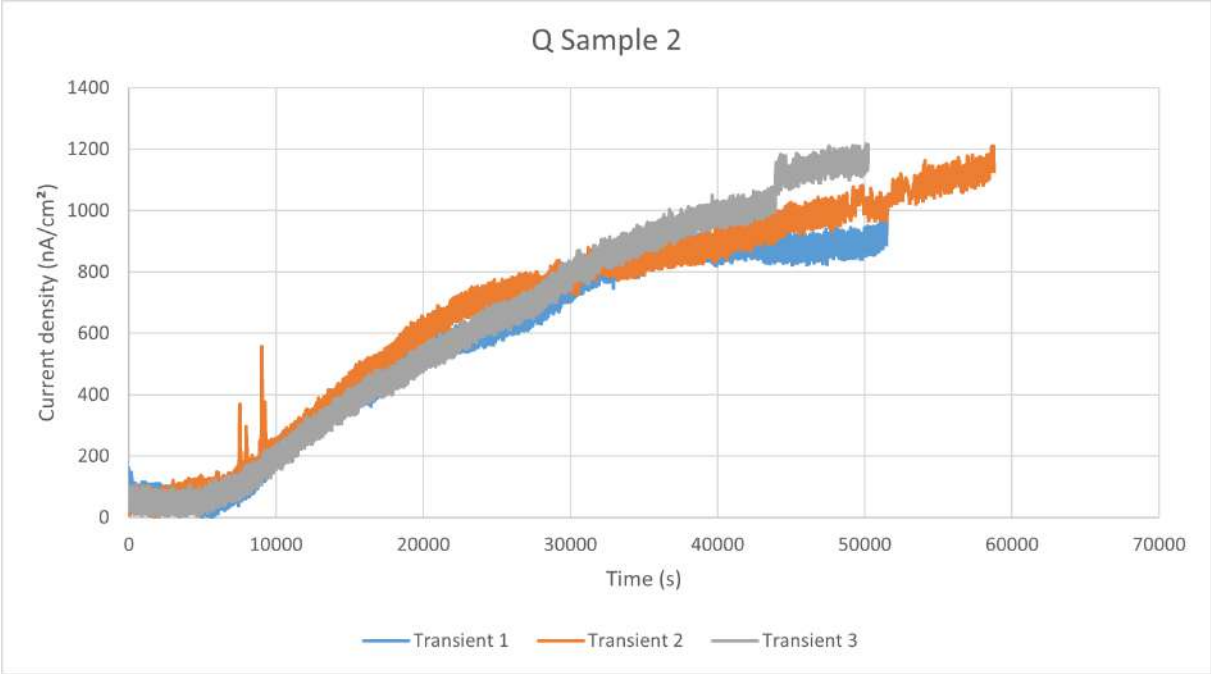


**Figure 4.8:** *The permeation transients for the 2nd Q sample.*

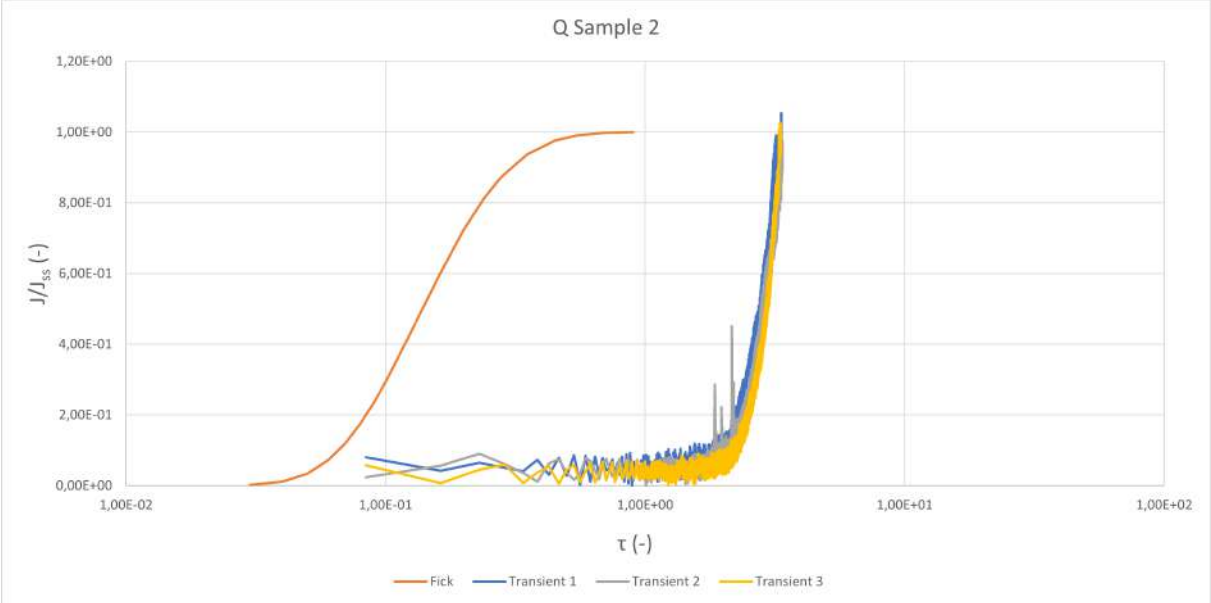


**Figure 4.9:** *The steady state permeation transients for the 2nd Q sample vs. normalized time.*

# 5 Discussion

## 5.1 The samples

### 5.1.1 B240

The second and third transient displays a rise similar to the first transient, which is indicative that little or no irreversible trapping happens in the material. However, it should be noted that no B240 sample passed all three runs (see table 5.1), which is the reason why the B240 transients are from different samples. The regular permeation transient curves are therefore not of good quality, and the reader is referred to the steady state permeation transients shown in figure 4.3 which takes differences of sample properties into account (including sample thickness). The final steady state achieved after charging is lower for transient 2 and 3. Comparing the transients to the Fick curve does indicate significant reversible trapping.

### 5.1.2 B280

B280's charging curves started roughly around the same time, which suggests that there are few or no irreversible traps within the material, but seeing as the curve is steeper than Fick's curve, it can be concluded that reversible trapping occurs[19]. The steady state flux was also found to be similar to B240, but the effective diffusion coefficient was the lowest of all 4 microstructures. B280 had more issues with charging as time went on. It is unclear what might have caused the irregularities in charging, as the charging curve became less predictable – one example of this is shown in plot 4.4, where the irregularities would present itself after about 30000 seconds into charging for each transient.

### 5.1.3 QT440

Interestingly, QT440 has similar charging transients to B240, despite a much lower content of retained austenite and a martensitic structure. It is natural to conclude that a lower amount of retained austenite and more martensite results in a higher diffusion[4]. However, the role of cementite is unclear. Some studies claim cementite increases the hydrogen embrittlement resistance within steels and act as an excellent hydrogen trapping site[28–30]. On the contrary, other studies have found the opposite to be the case, where "both the solubility and diffusivity of hydrogen in pure cementite are very low,

although the presence of vacancies or off-stoichiometric cementite will greatly increase the hydrogen solubility, while inhibiting the diffusivity"[31]. Nevertheless, it is difficult to make any definitive comments on the role of cementite without further research into it. The steady state diffusion flux was found to be higher than for other microstructures, with $t_{lag}$ being significantly lower as well. The steady state current and $D_{eff}$ were slightly higher for any other sample. The samples did not show any conclusive signs of irreversible trapping, but reversible trapping was discovered, as the curve incline is steeper than its Fick counterpart[19].

### 5.1.4 Q

A very low steady state flux was noted for the Q samples. The $t_{lag}$ values are comparable to B280. The microstructure does not have any iron carbides, but contains martensite with approximately 16% retained austenite. As mentioned previously there were slight variations in when the transients begun for Q. It is, however, not enough to conclude any irreversible trapping, as the differences are not consequent and appear random in nature. The steady state permeation transients do once again indicate reversible trapping, as the normalized permeation transients are steeper than the ideal Fick's curve[19].

### 5.1.5 General trends

Every microstructure had very little or no irreversible trapping, and every microstructure also showed signs of reversible trapping. There were slight differences in the hydrogen flux found for the microstructures. The QT440 steel, which contains tempered martensite and a smaller amount of retained austenite, had the highest hydrogen diffusivity, while the Q microstructure, only containing martensite and greater amounts of retained austenite, had the lowest diffusivity. As high martensite steels generally have higher diffusivity than austenite[4], the results are mostly what is to be expected compared to theory.

Permeation generally started after approximately 3000-10000 seconds for the samples after charging begun, but a large difference in charge time required for permeation to occur was observed between the different microstructures.

A hardness test was also performed to ensure that hydrogen embrittlement would be

relevant for our samples - a hardness greater than 32 HRC (310 HV) would confirm this[10]. The results of the hardness tests are seen in table 4.2.

## 5.2 Issues and challenges

### 5.2.1 Transients

Several runs had issues – and despite efforts to correct these issues, some faults lead to errors with the data. A colour code has been used to mark each run and its data validity in table 5.1. Valid sample data for one sample of each microstructure have been included in the results, but consecutive runs are to some extent dependent on the former run being valid, which poses an issue for the validity of the data for B240. The other results can be found in the appendix. The most significant issue with the experiment were general cell leaks. The gasket design was not the best and would intermittently leak.

| Microstructure | Transient 1 | Transient 2 | Transient 3 | Comments |
|---|---|---|---|---|
| B240 1 | ● | ● | ● | 1st run without thiourea |
| B240 2 | ● | ● | ● | 1st run without thiourea |
| B240 3 | ● | ● | ● | Failure 2nd run |
| B280 1 | ● | ● | ● | |
| B280 2 | ● | ● | ● | Leak 3rd run |
| B280 3 | ● | ● | ● | Strange results 2nd and 3rd run |
| QT440 1 | ● | ● | ● | |
| QT440 2 | ● | ● | ● | |
| QT440 3 | ● | ● | ● | |
| Q 1 | ● | ● | ● | |
| Q 2 | ● | ● | ● | |
| Q 3 | ● | ● | ● | 3rd run has strange results |

**Table 5.1:** *Every experimental run with its assessment of validity. Legend: Red = Failed, Yellow = Passed, but with strange results/after a failed run, Green = Passed, no issues*

Unlike the project thesis[32], much less jagged behaviour was observed for this run, but it is noted that the curves seems to have a lot of noise - for Q this noise is at $\pm 50nA$, and follows the curve. A plausible explanation to this noise might be related to the charging current being too high which can contribute to unsteady conditions. Previously, a $-1050$ mV charge potential was applied, but it was decided to increase this to ensure permeation. In this thesis a current of $-1$ mA/cm$^2$ was applied instead, causing a charge potential of around $-1400$ mV. With thiourea it will most likely be sufficient with a lower charge potential, but it should be noted that the permeation time is still very long compared to

many other permeation studies perfomed[27, 33, 34]. It is therefore concluded that this alloy in particular is very resistant against permeation compared to many other steels.

The diffusion coefficient $D_{eff}$ may be affected by using standard parameters for $D_O$ and $E_l$, which are intended for pure BCC iron. Realistically, it is difficult to find fitting constants for $D_0$ and $E_l$, and it is adviced to perform a separate study into finding better fitting constants for each microstructure. The austenitic phases possess an FCC structure, whereas martensite has a BCT structure, and it is therefore natural to conclude that the austenitic phases have lower diffusion than both martensite and ferrite, as previously mentioned in the theory section. Most values for $D_{eff}$ are validated by using the formula for minimum effective diffusivity in steel. The formula was proposed by Boellinghaus et al.[35]:

$$D_{min} = 8.8 * 10^{-15}(T - 273)^{2.2285} m^2 s^{-1} \tag{5.1}$$

which provides information about what is the minimum logical diffusivity at a given temperature. For this thesis, $D_{min}$ was found to be $9.53 * 10^{-12}$ $m^2s^{-1}$ at a temperature of 23°C, which is lower than the lowest diffusivity found for any of the samples, except B280 transient 3. It is therefore believed that the diffusivity value found here is improbable.

### 5.2.2 Issues

The current leaks did not occur between the electrolytes themselves, or around the gasket of the sample itself, as was the case with the project thesis[32] - but rather at the gasket which was intended to seal off the compartment at the Teflon opening size reduction fitting. No inner gasket leaks were recorded. The best way of solving this problem would have been to produce a new permeation cell - however, with the economical constraints of this thesis, the opening size reduction fitting solution was implemented. The main issue was therefore linked to electrolyte leaking from the cell itself, and therefore reducing contact with the counter- and working electrode. The cell was checked for dripping after electrolyte was added, but in some cases the change in wall pressure from holding the cell to putting it down could cause a leak! As a result, the cell was replaced by another similar cell without the need to use a special fitting, for QT440 and Q, which stopped the leaks without affecting the experiment.

The potentiostats posed another issue and could lead to errors while running. In one instance, a sudden voltage spike was detected, causing one potentiostat to stop running. Another run was cancelled due to a generic error message from the potentiostat. These examples are two of several cases where the potentiostats either failed or caused issues with the readings. Several fixes were attempted, including potentiostat calibration – however, sometimes the potentiostat simply needed to be rebooted, and the reason behind the problem remained unknown.

Sample corrosion was a huge issue in the previous thesis[32]. This experiment therefore utilized 0.1M NaOH in both chambers after some research[36]. Surface corrosion was still detected, but the issue was much less significant this time, compared to former experiments where 3.5wt% NaCl in H2O was used as an electrolyte. Thus, evidence exists indicating that corrosion had little or no effect on the results.

Other issues, like a slightly large reference electrode impedance being recorded (up to 10000 Ohm), might have had some effect on the experiment. Reference electrodes were replaced when a high impedance was detected, but values up to 5000 Ohm were tolerated. Unsteady surface conditions might cause a greater disturbance of the results. Several points have been noted as to why this might be the case. pH was not recorded, although, a change in pH may occur as a result of the hydrogen permeation and could explain the continuous rise of the transients after post-diffusion steady state was obtained, as well as the abrupt curve variations as seen i.e. in sample Q 1. Another explanation of this phenomenon is given by Zakroczymski et al.[36, 37], who showed that the surface barrier which the cathodic charging process aims to remove might have still been present to some degree. However, this lies beyond the scope of this thesis, and it is not believed that this has had any significant impact on the results found in 3.

Trap occupancy might also affect the diffusion coefficient, which therefore might make the diffusion coefficient a varying parameter as a function of the trap occupancy[38]. However, it is assumed that the samples do not have a concentration of reversible trapped significant enough to render a diffusion coefficient invalid. An accurate value of trap occupancy requires the experiment to be conducted at several temperatures – this has

not been performed, and therefore, only general comments on trapping have been made in this thesis.

### 5.2.3 Thiourea

The first two runs for B240 were performed without thiourea – one curve is appended below to show why thiourea was used. The transient were significantly more difficult to interpret without thiourea.

Thiourea is, as mentioned in section 2.1, a hydrogen recombination poison. The hydrogen is therefore forced through the sample instead, which reduces the experiment time and vastly increases the intensity of the charging curve. As seen for figure 5.1, the curve is hard to define due to the noise in the experiment, and it seems like the current density only increases about 100 nA upon permeation – however, it is difficult to determine whether this is actual permeation or a result of the noise in the experiment. By using thiourea, penetration occurred in only a few hours and a well defined transient with a total increase of around 1-2 µA was observed.

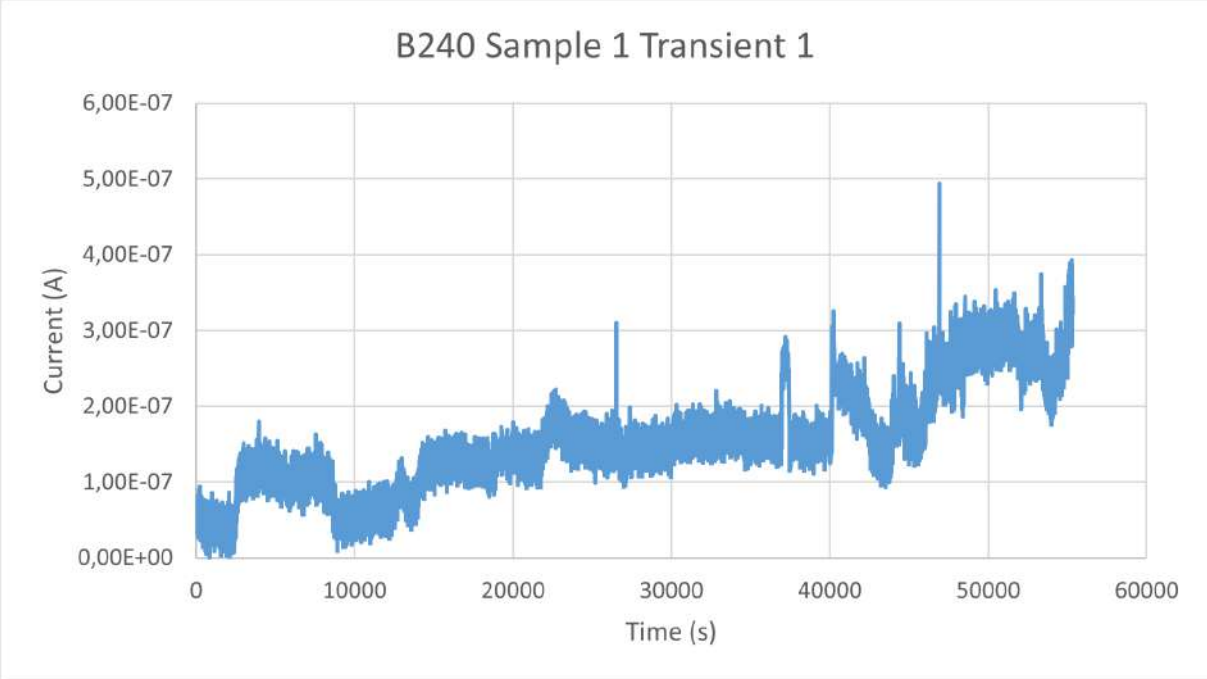


**Figure 5.1:** *B240 sample 1 transient 1. Noise and irregularities makes it difficult to determine any permeation transient.*

# 6 Conclusion & future work

The transients which have been found are of useful quality, and the data found suggest that there are only slight differences between the four microstructures tested. All microstructures seemed to have significant reversible trapping, but there were no evidence of irreversible trapping. QT440 had a larger flux than the other samples, which could be linked to its martensite content. Experimental problems included cell leaks were the most difficult to deal with, but also issues with the potentiostats did lead to problems. Addition of thiourea has significantly improved the quality of the data, as it would most likely be impossible to get good readings without it. Replacing the 3.5wt% NaCl solution with 0.1M NaOH in the cathodic chamber also helped the corrosion issues from the previous thesis. Future work with these results should be put into finding better constants for $D_l$ and $E_l$ instead of using pure BCC iron values. It would also be advisable to look further into the charging current/potential as previously mentioned, and possibly also perform diffusion tests on the D microstructure. A thermal desorption spectometry would also be recommended, to study the depletion of hydrogen from the microstructures, and tensile testing of specimens of the tested microstructures would provide valuable information about the impact of hydrogen embrittlement.

# 7 Acknowledgements

This thesis is part of a cooperation between SINTEF, Kverneland Group and the author, a master student at the Norwegian University of Science and Technology (NTNU). The author would like to thank Andreas Erbe for his role as a supervisor, as well as Erlend Sølvberg, Erik Aas Koren and Iman Taji for their valuable support in producing the results of this thesis.

# Bibliography


[1] D. Hardie, E.A. Charles, and A.H. Lopez. "Hydrogen embrittlement of high strength pipeline steels". In: *Corrosion Science* 48.12 (2006), pp. 4378–4385. ISSN: 0010-938X. DOI: https://doi.org/10.1016/j.corsci.2006.02.011. URL: https://www.sciencedirect.com/science/article/pii/S0010938X06000710.

[2] Yu-Tung Hsu et al. "Hydrogen-induced embrittlement of nickel-chromium-molybdenum containing HSLA steels". In: *Journal of the Chinese Institute of Engineers* 43.1 (2020), pp. 58–66. DOI: 10.1080/02533839.2019.1676659. eprint: https://doi.org/10.1080/02533839.2019.1676659. URL: https://doi.org/10.1080/02533839.2019.1676659.

[3] Stan Lynch. "Hydrogen embrittlement phenomena and mechanisms". In: *Corrosion Reviews* 30.3-4 (2012), pp. 105–123. DOI: doi:10.1515/corrrev-2012-0502. URL: https://doi.org/10.1515/corrrev-2012-0502.

[4] Alan Turnbull. "Hydrogen diffusion and trapping in metals". In: 2012.

[5] C.M. Younes et al. "Influence of hydrogen content on the tensile properties and fracture of austenitic stainless steel welds". In: *International Journal of Hydrogen Energy* 38.11 (2013), pp. 4864–4876. ISSN: 0360-3199. DOI: https://doi.org/10.1016/j.ijhydene.2012.11.016. URL: https://www.sciencedirect.com/science/article/pii/S0360319912024615.

[6] Harshad Kumar Dharamshi Hansraj Bhadeshia. "Prevention of Hydrogen Embrittlement in Steels". In: *ISIJ International* 56.1 (2016), pp. 24–36. DOI: 10.2355/isijinternational.ISIJINT-2015-430.

[7] Fengping Luo et al. "Effects of lattice strain on hydrogen diffusion, trapping and escape in bcc iron from ab-initio calculations". In: *International Journal of Hydrogen Energy* (2022). ISSN: 0360-3199. DOI: https://doi.org/10.1016/j.ijhydene.2022.11.206. URL: https://www.sciencedirect.com/science/article/pii/S0360319922055240.

[8] Jun Song and W. A. Curtin. "Atomic mechanism and prediction of hydrogen embrittlement in iron". In: *Nature Materials* 12.2 (2013), pp. 145–151. ISSN: 1476-4660. DOI: 10.1038/nmat3479. URL: https://doi.org/10.1038/nmat3479.

[9] R A Oriani. "Hydrogen Embrittlement of Steels". In: *Annual Review of Materials Science* 8.1 (1978), pp. 327–357. DOI: 10.1146/annurev.ms.08.080178.001551. eprint: https://doi.org/10.1146/annurev.ms.08.080178.001551. URL: https://doi.org/10.1146/annurev.ms.08.080178.001551.

[10] Jonathan A. Lee. "Hydrogen Embrittlement". In: *NASA* (2016).

[11] Haiyang Yu, Alan Cocks, and Edmund Tarleton. "Discrete dislocation plasticity HELPs understand hydrogen effects in bcc materials". In: *Journal of the Mechanics and Physics of Solids* 123 (2019). The N.A. Fleck 60th Anniversary Volume, pp. 41–60. ISSN: 0022-5096. DOI: https://doi.org/10.1016/j.jmps.2018.08.020. URL: https://www.sciencedirect.com/science/article/pii/S002250961830574X.

[12] Michael D. Dolan et al. "Hydride phase equilibria in V–Ti–Ni alloy membranes". In: *Journal of Alloys and Compounds* 622 (2015), pp. 276–281. ISSN: 0925-8388. DOI: https://doi.org/10.1016/j.jallcom.2014.10.081. URL: https://www.sciencedirect.com/science/article/pii/S0925838814025018.

[13] Laura Vergani et al. "Hydrogen Effect on Fatigue Behavior of a Quenchedtempered Steel". In: *Procedia Engineering* 74 (2014). XVII International Colloquium on Mechanical Fatigue of Metals (ICMFM17), pp. 468–471. ISSN: 1877-7058. DOI: https://doi.org/10.1016/j.proeng.2014.06.299. URL: https://www.sciencedirect.com/science/article/pii/S1877705814008698.

[14] Huiyun Tian et al. "Electrochemical corrosion, hydrogen permeation and stress corrosion cracking behavior of E690 steel in thiosulfate-containing artificial seawater". In: *CORROSION SCIENCE* 144 (2018), pp. 145–162. ISSN: 0010-938X. DOI: 10.1016/j.corsci.2018.08.048.

[15] Chengshuang Zhou et al. "Effect of pre-strain on hydrogen embrittlement of metastable austenitic stainless steel under different hydrogen conditions". In: *INTERNATIONAL JOURNAL OF HYDROGEN ENERGY* 44.47 (2019), pp. 26036–26048. ISSN: 0360-3199. DOI: 10.1016/j.ijhydene.2019.08.046.

[16] Qian Yan et al. "Hydrogen trapping and hydrogen embrittlement in 15-5PH stainless steel". In: *Corrosion Science* 205 (2022), p. 110416. ISSN: 0010-938X. DOI: https://doi.org/10.1016/j.corsci.2022.110416. URL: https://www.sciencedirect.com/science/article/pii/S0010938X22003341.

[17] SLI Chan. "Hydrogen trapping ability of steels with different microstructures". In: *JOURNAL OF THE CHINESE INSTITUTE OF ENGINEERS* 22.1 (1999), pp. 43–53. ISSN: 0253-3839. DOI: 10.1080/02533839.1999.9670440.

[18] Xiaobing Cheng et al. "Hydrogen diffusion and trapping in V-microalloyed mooring chain steels". In: *MATERIALS LETTERS* 213 (2018), pp. 118–121. ISSN: 0167-577X. DOI: 10.1016/j.matlet.2017.11.029.

[19] International Organization for Standards. "Method of measurement of hydrogen permeation and determination of hydrogen uptake and transport in metals by an electrochemical technique". In: *International Organization for Standards* 2 (2019).

[20] American Society for Testing and Materials. "Standard Practice for Evaluation of Hydrogen Uptake, Permeation, and Transport in Metals by an Electrochemical Technique". In: *American Society for Testing and Materials* (2018).

[21] BJ BERKOWITZ et al. "HYDROGEN DISSOCIATION POISONS AND HYDROGEN EMBRITTLEMENT". In: *SCRIPTA METALLURGICA* 10.10 (1976), pp. 871–873. ISSN: 0036-9748. DOI: 10.1016/0036-9748(76)90203-9.

[22] P. Manolatos and M. Jerome. "A thin palladium coating on iron for hydrogen permeation studies". In: *Electrochimica Acta* 41.3 (1996), pp. 359–365. ISSN: 0013-4686. DOI: https://doi.org/10.1016/0013-4686(95)00379-7. URL: https://www.sciencedirect.com/science/article/pii/0013468695003797.

[23] P. Manolatos et al. "The electrochemical permeation of hydrogen in steels without palladium coating. Part I: Interpretation difficulties". In: *Corrosion Science* 37.11 (1995), pp. 1773–1783. ISSN: 0010-938X. DOI: https://doi.org/10.1016/0010-938X(95)00079-Y. URL: https://www.sciencedirect.com/science/article/pii/0010938X9500079Y.

[24] P Bruzzoni, R.M Carranza, and J.R Collet Lacoste. "Influence of palladium films on hydrogen gas entry into iron: a study by electrochemical impedance spectroscopy". In: *International Journal of Hydrogen Energy* 25.1 (2000), pp. 61–65. ISSN: 0360-3199. DOI: https://doi.org/10.1016/S0360-3199(99)00010-5. URL: https://www.sciencedirect.com/science/article/pii/S0360319999000105.

[25] A. Turnbull and M.W. Carroll. "The effect of temperature and H2S concentration on hydrogen diffusion and trapping in a 13% chromium martensitic stainless steel in acidified NaCl". In: *Corrosion Science* 30.6 (1990), pp. 667–679. ISSN: 0010-938X.

DOI: https://doi.org/10.1016/0010-938X(90)90031-Y. URL: https://www.sciencedirect.com/science/article/pii/0010938X9090031Y.

[26] N. Boes and H. Züchner. "Electrochemical methods for studying diffusion, permeation and solubility of hydrogen in metals". In: *Journal of the Less Common Metals* 49 (1976). Hydrogen in metals, pp. 223–240. ISSN: 0022-5088. DOI: https://doi.org/10.1016/0022-5088(76)90037-0. URL: https://www.sciencedirect.com/science/article/pii/0022508876900370.

[27] Hans Husby et al. "Effect of nickel on hydrogen permeation in ferritic/pearlitic low alloy steels". In: *International Journal of Hydrogen Energy* 43.7 (2018), pp. 3845–3861. ISSN: 0360-3199. DOI: https://doi.org/10.1016/j.ijhydene.2017.12.174. URL: https://www.sciencedirect.com/science/article/pii/S0360319917348954.

[28] M. Pinson et al. "The role of cementite on the hydrogen embrittlement mechanism in martensitic medium-carbon steels". In: *Materials Science and Engineering: A* 859 (2022), p. 144204. ISSN: 0921-5093. DOI: https://doi.org/10.1016/j.msea.2022.144204. URL: https://www.sciencedirect.com/science/article/pii/S0921509322015842.

[29] Wayne M. Robertson and Anthony W. Thompson. "Permeation measurements of hydrogen trapping in 1045 steel". In: *Metallurgical Transactions A* 11.4 (1980), pp. 553–557. ISSN: 2379-0180. DOI: 10.1007/BF02670691. URL: https://doi.org/10.1007/BF02670691.

[30] M. Pinson et al. "Investigation of the effect of carbon on the reversible hydrogen trapping behavior in lab-cast martensitic FeC steels". In: *Materials Characterization* 184 (2022), p. 111671. ISSN: 1044-5803. DOI: https://doi.org/10.1016/j.matchar.2021.111671. URL: https://www.sciencedirect.com/science/article/pii/S1044580321007932.

[31] Eunan J. McEniry, Tilmann Hickel, and Jörg Neugebauer. "Ab initio simulation of hydrogen-induced decohesion in cementite-containing microstructures". In: *Acta Materialia* 150 (2018), pp. 53–58. ISSN: 1359-6454. DOI: https://doi.org/10.1016/j.actamat.2018.03.005. URL: https://www.sciencedirect.com/science/article/pii/S1359645418301848.

[32] Christian Vågenes. "Hydrogen permeation in different microstructures of 66SiMnCrMo6-6-4 steel". In: (2022), pp. 1–20.

[33] Oluwole Kazum et al. "Hydrogen Permeation in Nanostructured Bainitic Steel". In: *Metallurgical and Materials Transactions A* 47.10 (2016), pp. 4896–4903. ISSN: 1543-1940. DOI: 10.1007/s11661-016-3677-2. URL: https://doi.org/10.1007/s11661-016-3677-2.

[34] O. Kazum, H. Beladi, and M. Bobby Kannan. "Hydrogen permeation in twinning-induced plasticity (TWIP) steel". In: *International Journal of Hydrogen Energy* 43.50 (2018), pp. 22685–22693. ISSN: 0360-3199. DOI: https://doi.org/10.1016/j.ijhydene.2018.10.121. URL: https://www.sciencedirect.com/science/article/pii/S0360319918333202.

[35] Th. Boellinghaus, H. Hoffmeister, and A. Dangeleit. "A scatterband for hydrogen diffusion coefficients in microalloyed and low carbon structural steels". In: *Welding in the World / Le Soudage dans le Monde* 35.2 (1995), pp. 149–149. ISSN: 0043-2288.

[36] T. Zakroczymski. "Permeability of iron to hydrogen cathodically generated in 0.1 M NaoH". In: *Scripta Metallurgica* 19.4 (1985), pp. 521–524. ISSN: 0036-9748. DOI: https://doi.org/10.1016/0036-9748(85)90126-7. URL: https://www.sciencedirect.com/science/article/pii/0036974885901267.

[37] T. Zakroczymski and Z. Szklarska-Smialowska. "Activation of the Iron Surface to Hydrogen Absorption Resulting from a Long Cathodic Treatment in NaOH Solution". In: *Journal of The Electrochemical Society* 132.11 (1985), p. 2548. DOI: 10.1149/1.2113621. URL: https://dx.doi.org/10.1149/1.2113621.

[38] A. Turnbull. "Perspectives on hydrogen uptake, diffusion and trapping". In: *International Journal of Hydrogen Energy* 40.47 (2015). Special issue on 1st International Conference on Hydrogen Storage, Embrittlement and Applications (Hy-SEA 2014), 26-30 October 2014, Rio de Janeiro, Brazil, pp. 16961–16970. ISSN: 0360-3199. DOI: https://doi.org/10.1016/j.ijhydene.2015.06.147. URL: https://www.sciencedirect.com/science/article/pii/S0360319915016766.

# A Further results

The data below has not been processed and refined to the same degree as the data in the thesis itself.

## A.1 B240

As mentioned previously, no sample had all three transients intact for B240. An alternative to the B240 curve appended under Results has been made, using the intact sample 1 curves: No other Fick curves were made for B240, as the results are slightly dubious.

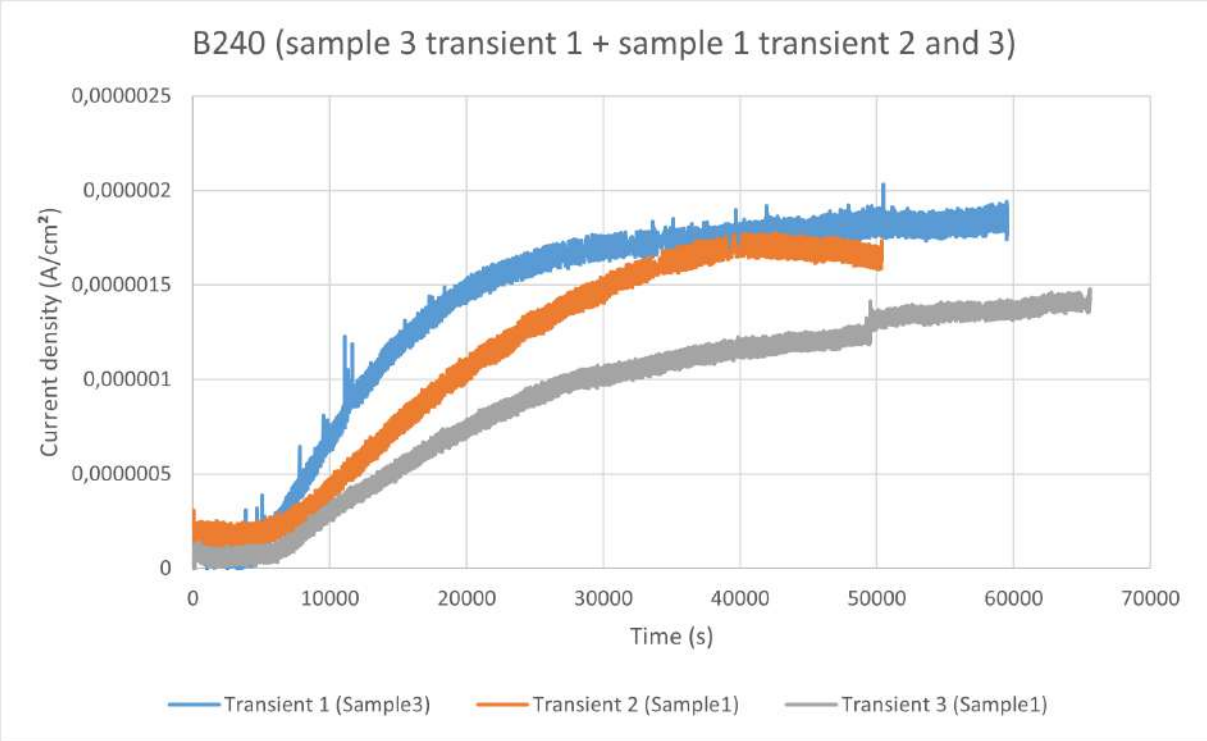


**Figure A.1:** *B240, sample 3 and 1. Each curve has had its pre-permeation steady state current subtracted from each data point.*

## A.2 B280

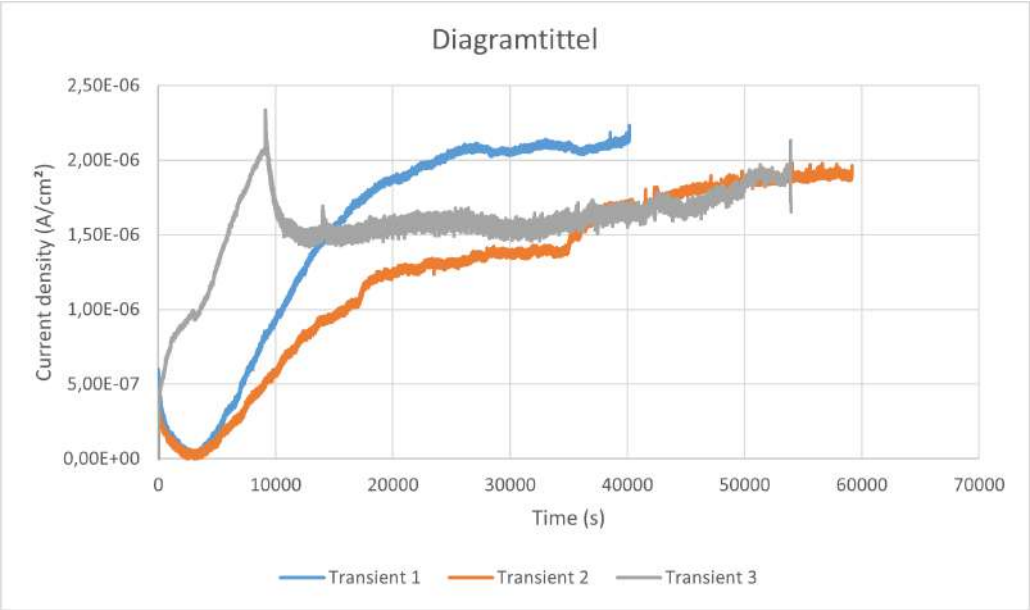


**Figure A.2:** *B280, sample 2. Each curve has had its pre-permeation steady state current subtracted from each data point. Transient 3 had failed.*

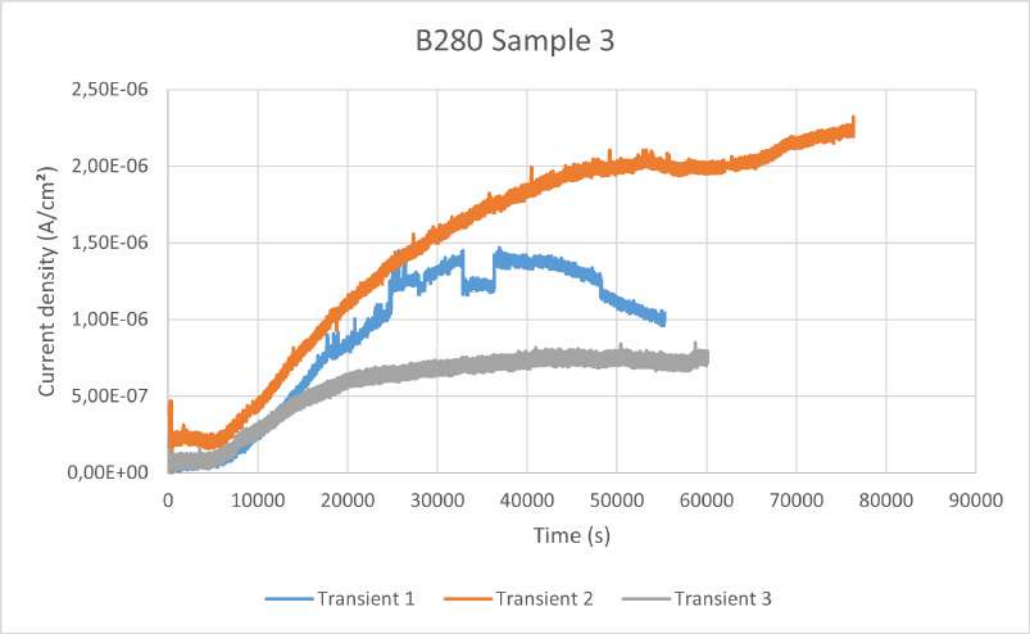


**Figure A.3:** *B280, sample 3. Each curve has had its pre-permeation steady state current subtracted from each data point. Strange curve behaviour.*

No Fick curves for the other B280 results, as these also were bad/dubious.

## A.3 QT440

The QT440 samples were the most successful of all samples.

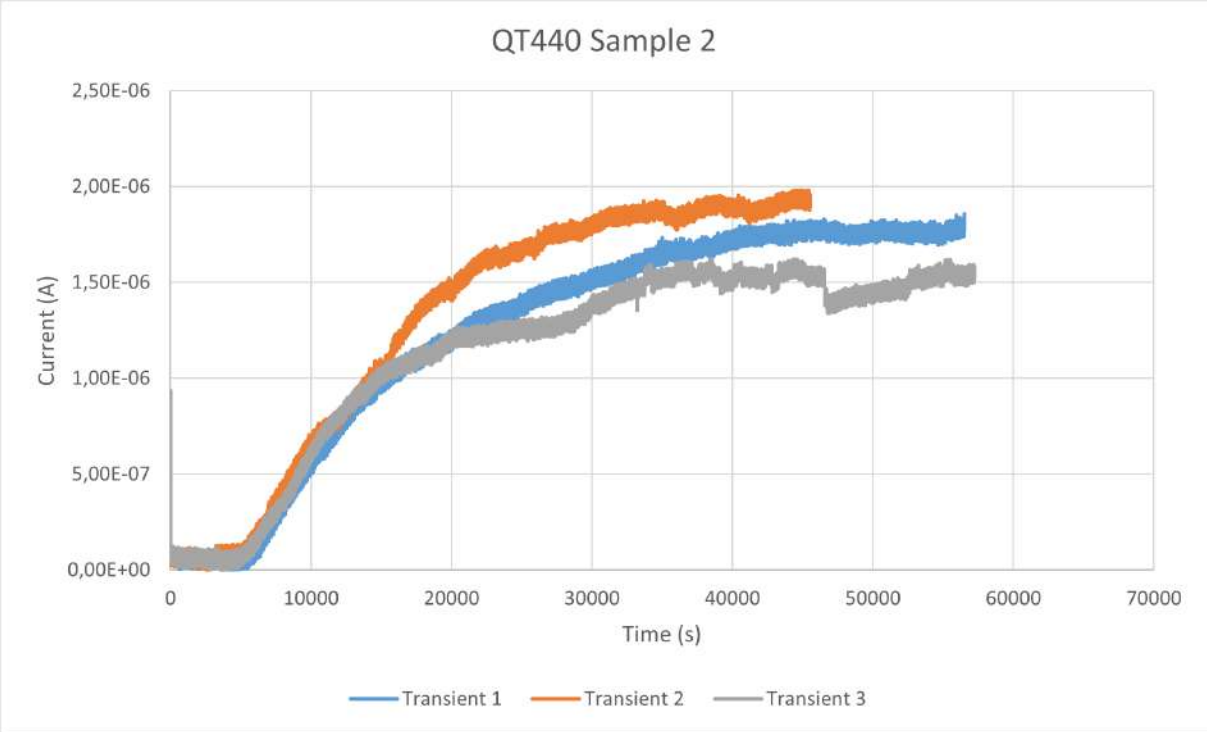


**Figure A.4:** *QT440, sample 2. Each curve has had its pre-permeation steady state current subtracted from each data point.*

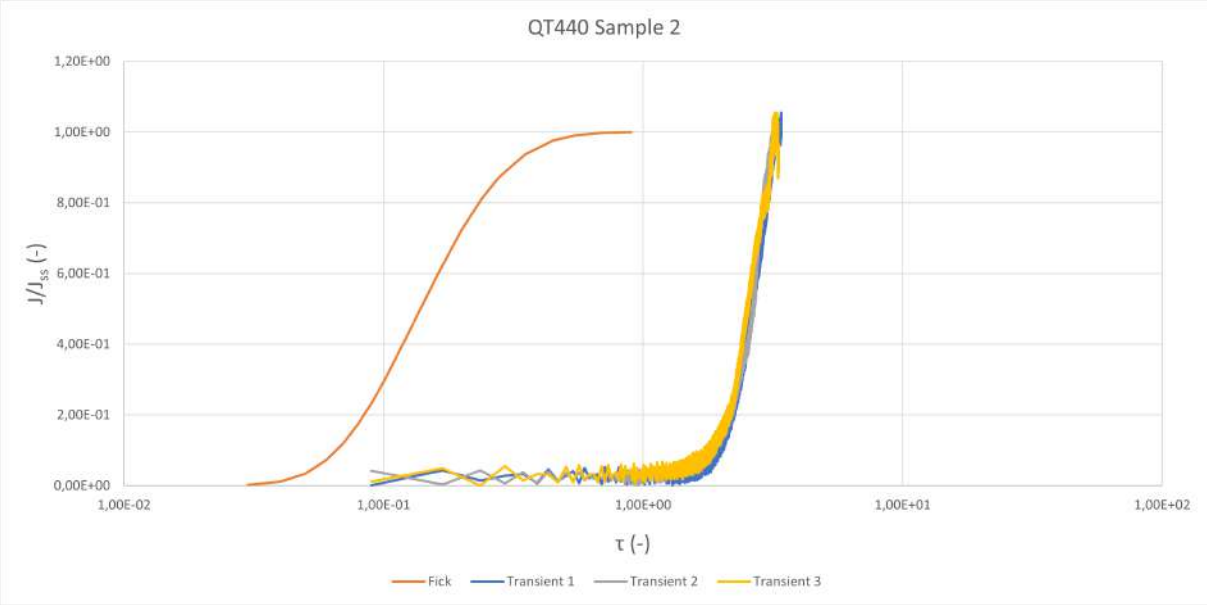


**Figure A.5:** *QT440, sample 2, Fick curve. Each curve has had its pre-permeation steady state current subtracted from each data point.*

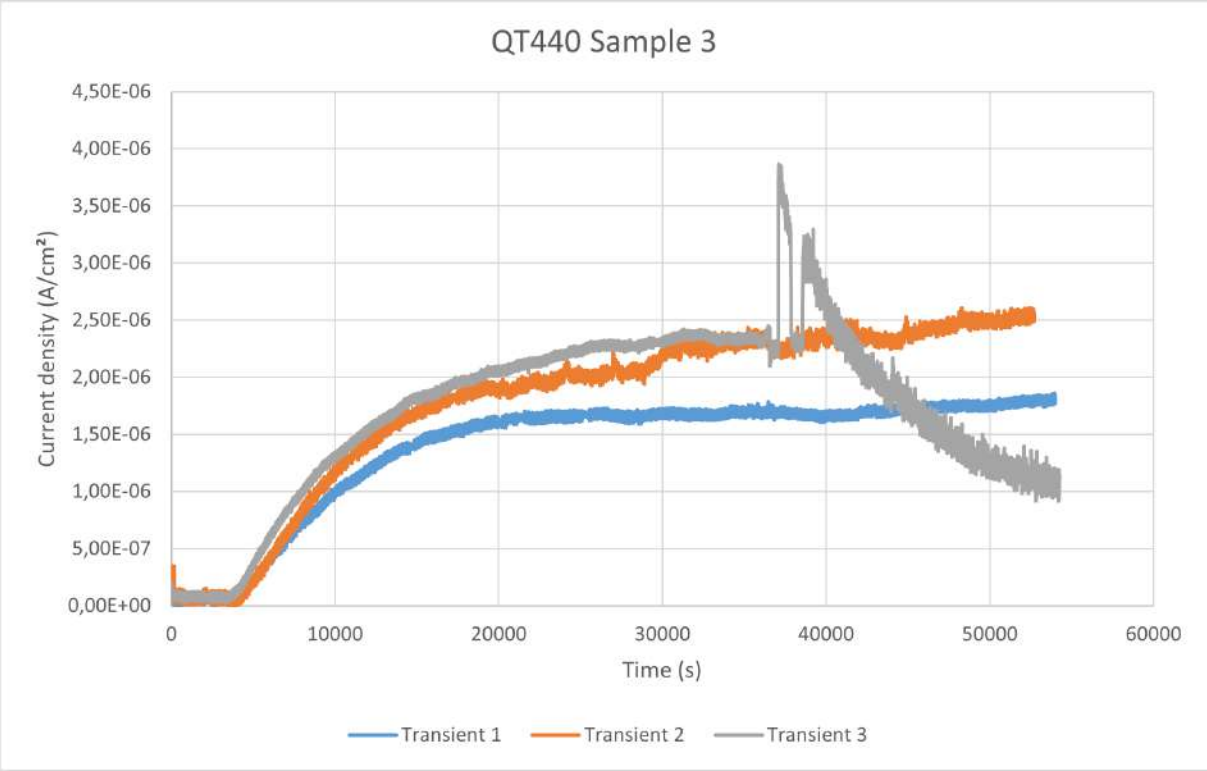


**Figure A.6:** *QT440, sample 3. Each curve has had its pre-permeation steady state current subtracted from each data point.*

## A.4 Q

The Q results were good, with an exception of sample 3 transient 3. It is not clear what might have happened to this curve.

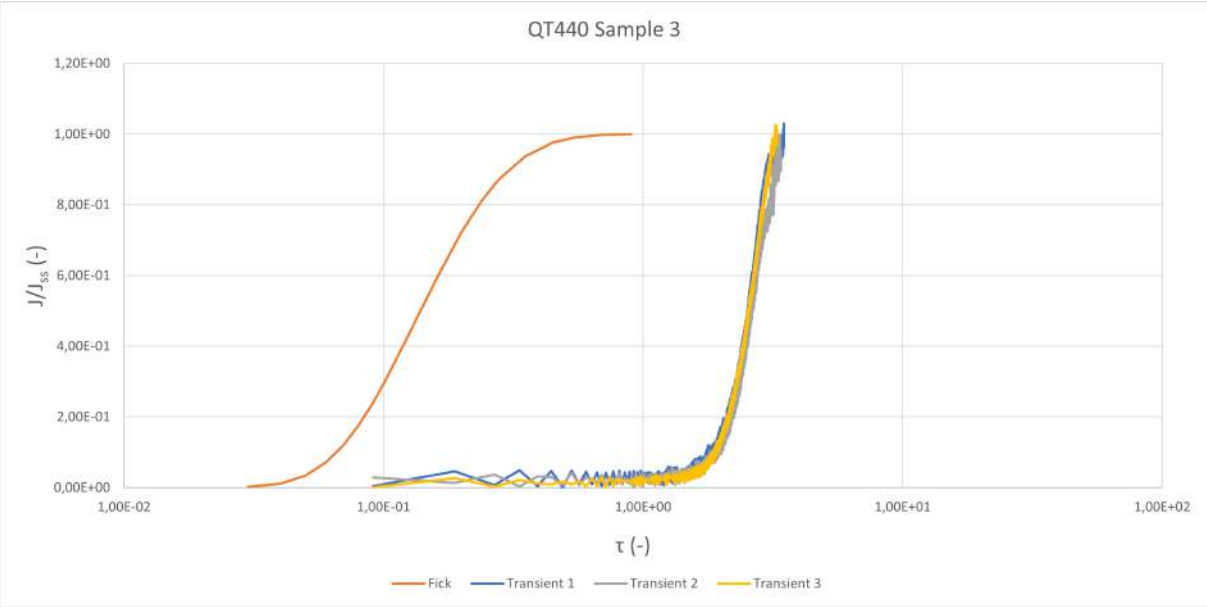


**Figure A.7:** *QT440, sample 3, Fick curve. Each curve has had its pre-permeation steady state current subtracted from each data point. Transient 3 exhibited strange behaviour after 35000 seconds, but it is not believed to affect the transient itself.*

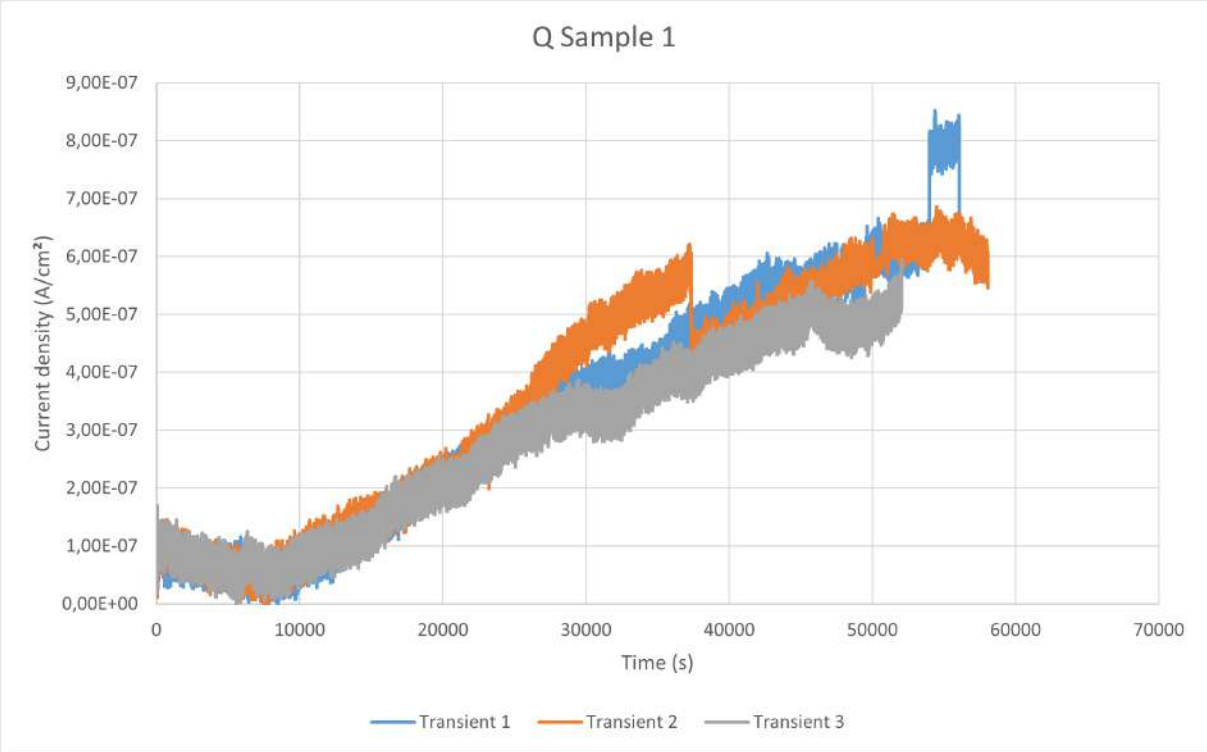


**Figure A.8:** *Q, sample 1. Each curve has had its pre-permeation steady state current subtracted from each data point.*

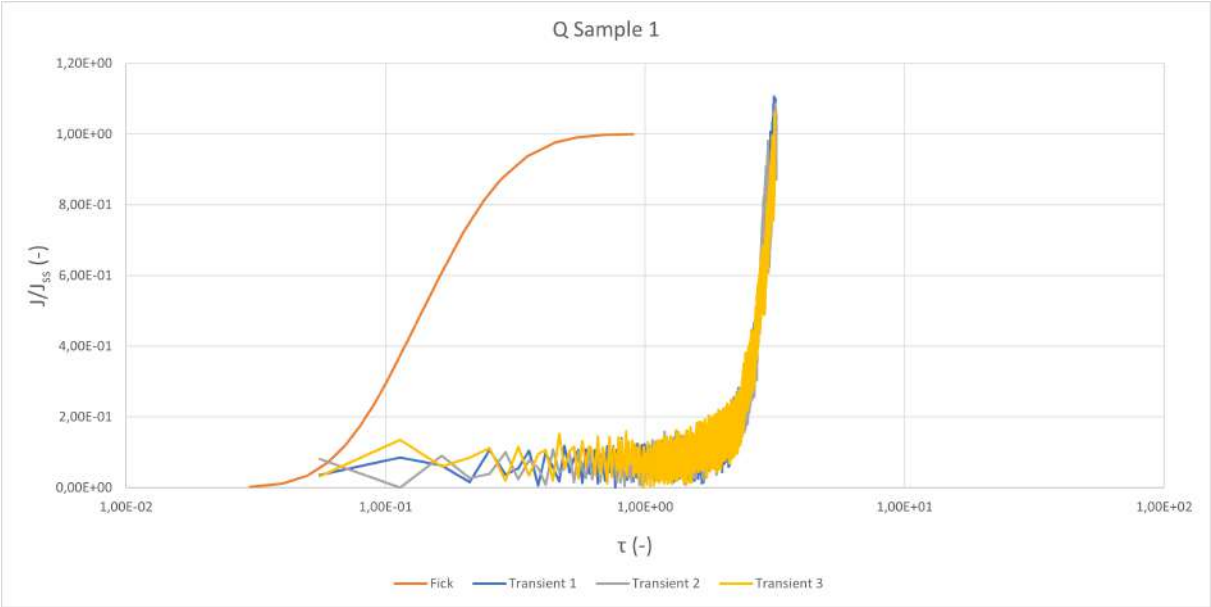


**Figure A.9:** *Q, sample 1, Fick curve. Each curve has had its pre-permeation steady state current subtracted from each data point. A very jagged transient curve at the beginning was noted here.*

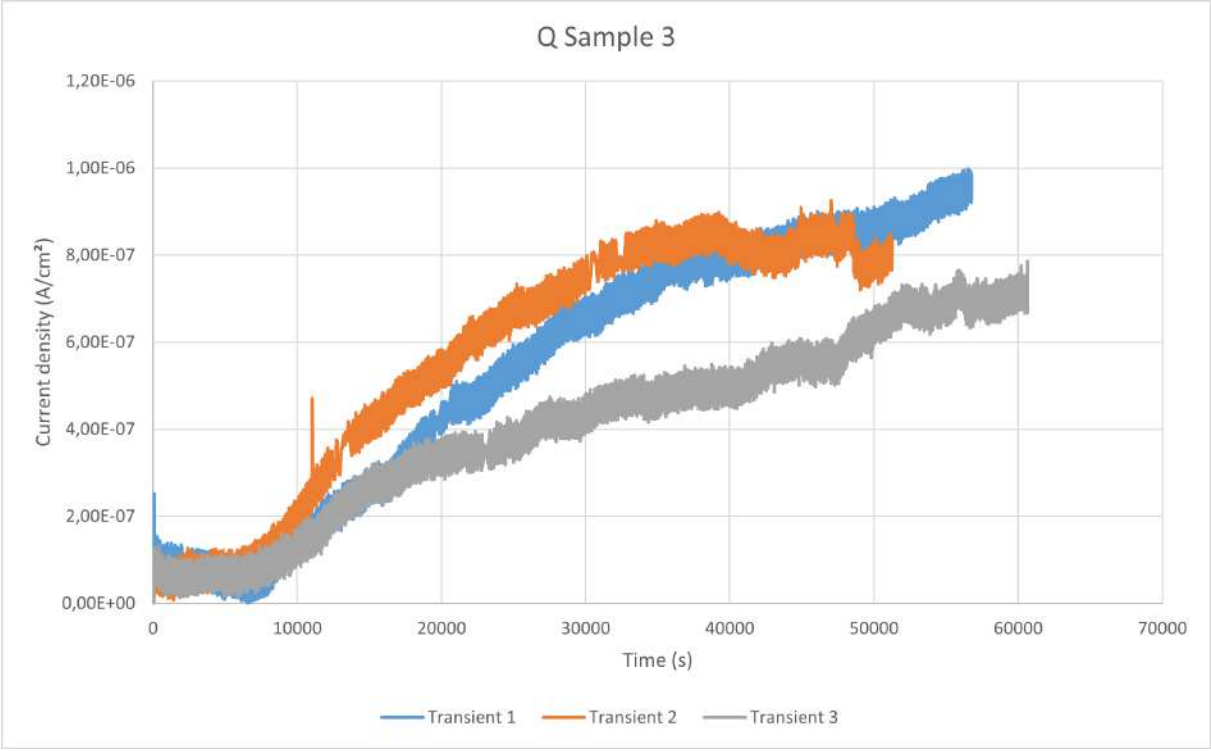


**Figure A.10:** *Q, sample 3. Each curve has had its pre-permeation steady state current subtracted from each data point. The third curve had a very different transient, and it is believed that the data is slightly dubious.*

# B Microscopy images

New microscopy images were taken of all samples, as a new microstructure had been introduced and the old ones were not of the best quality.

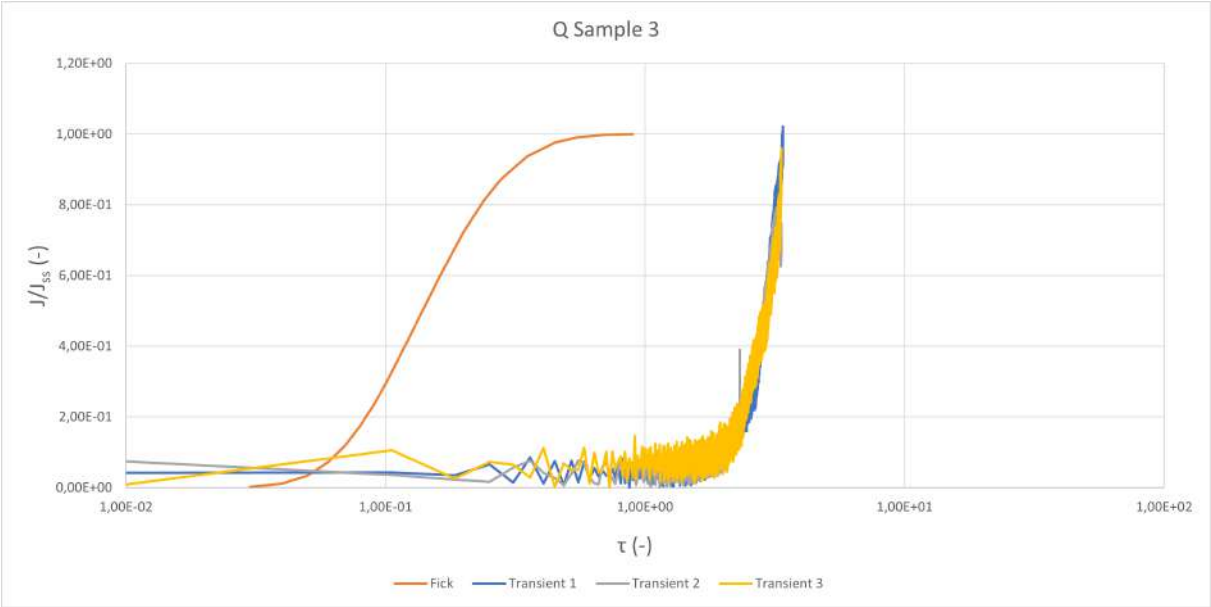


**Figure A.11:** *Q, sample 3, Fick curve. Each curve has had its pre-permeation steady state current subtracted from each data point. A very jagged transient curve at the beginning was noted here.*

## B.1 500x

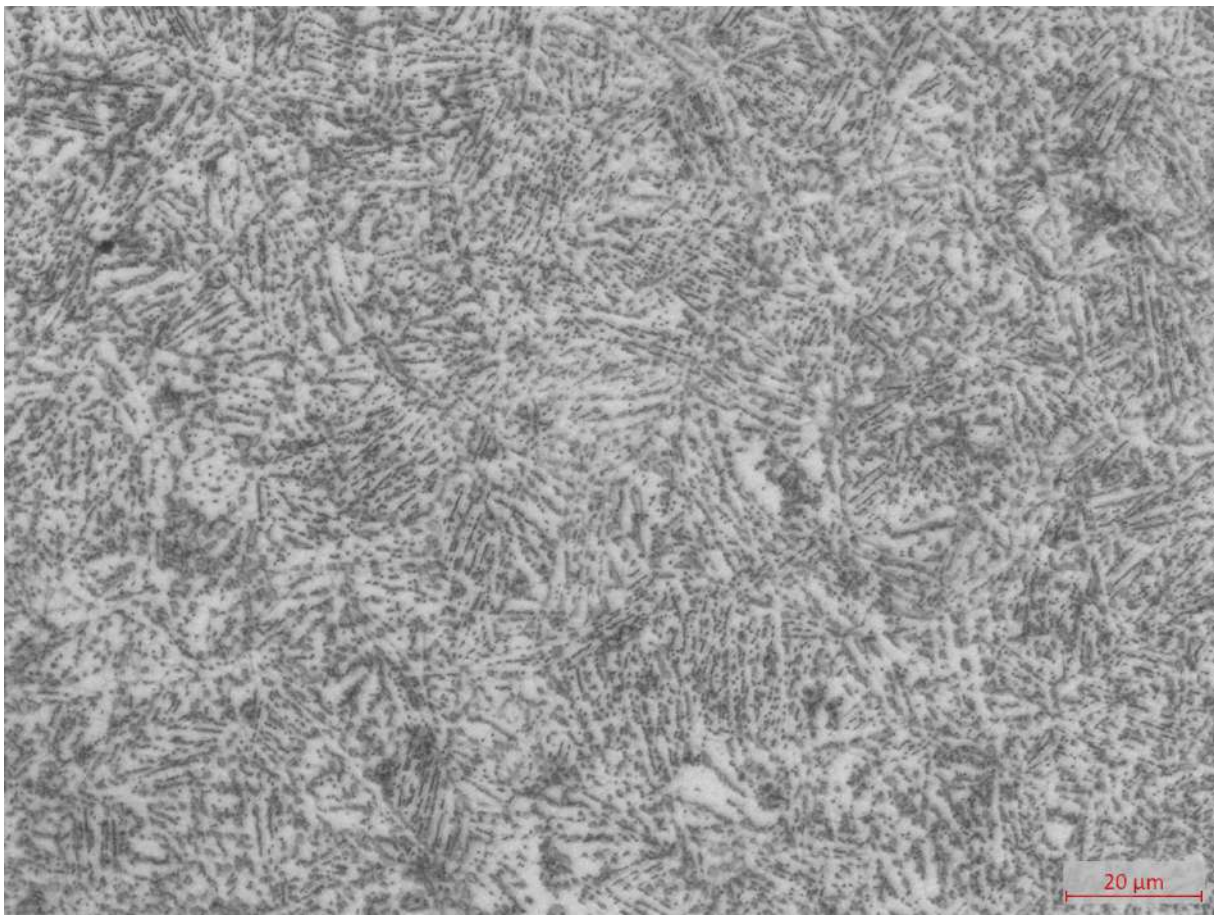


**Figure B.1:** *D, 500x magnification*

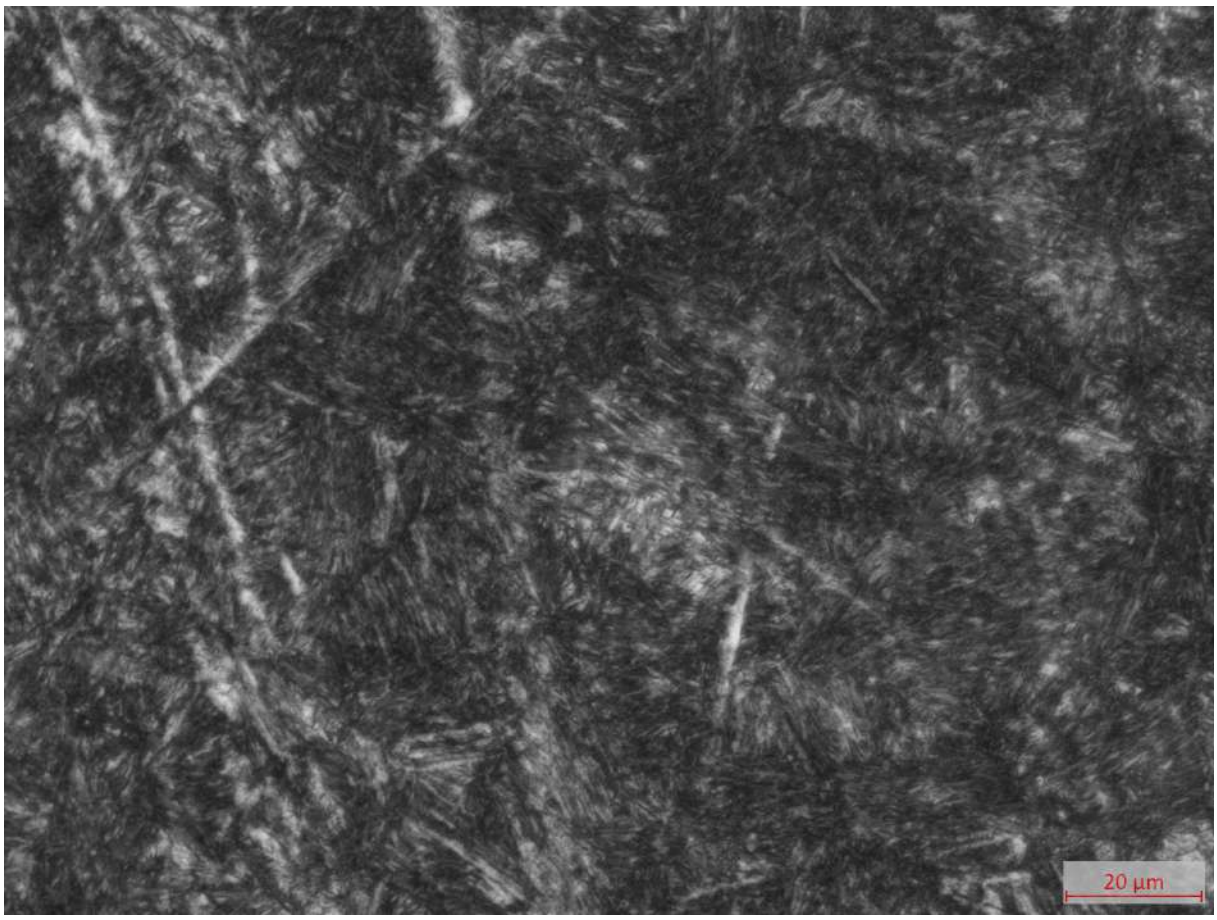


**Figure B.2:** *B240, 500x magnification*

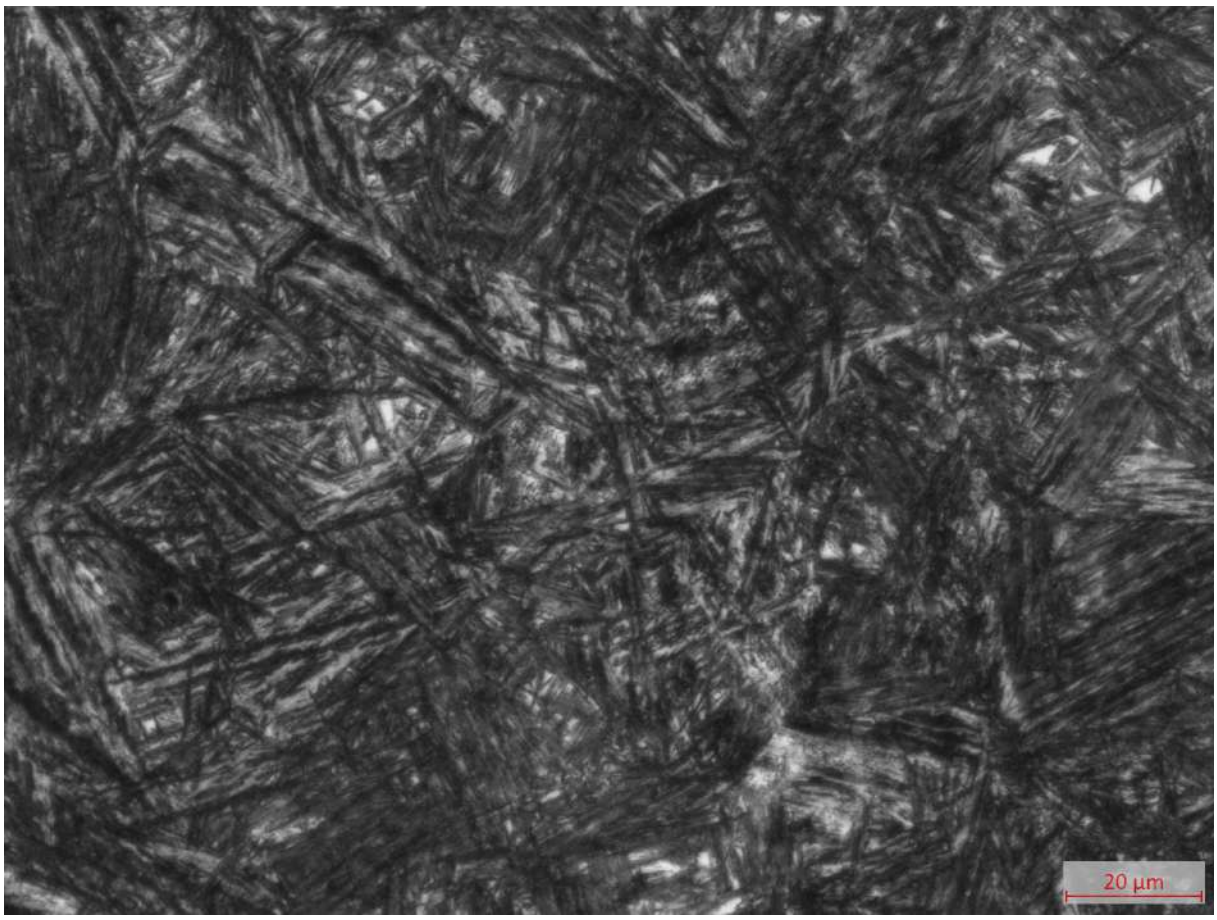


**Figure B.3:** *B280, 500x magnification*

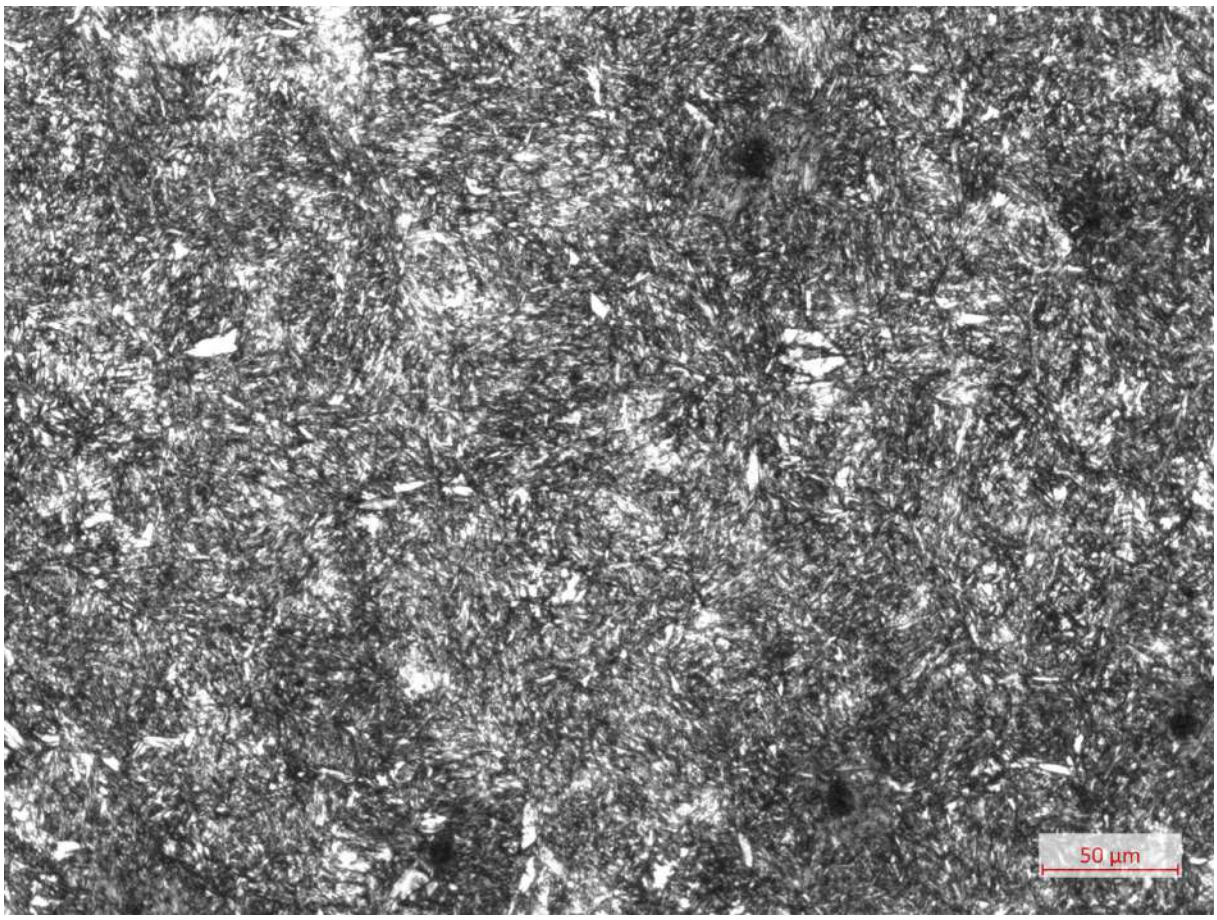


**Figure B.4:** *QT440, 500x magnification*

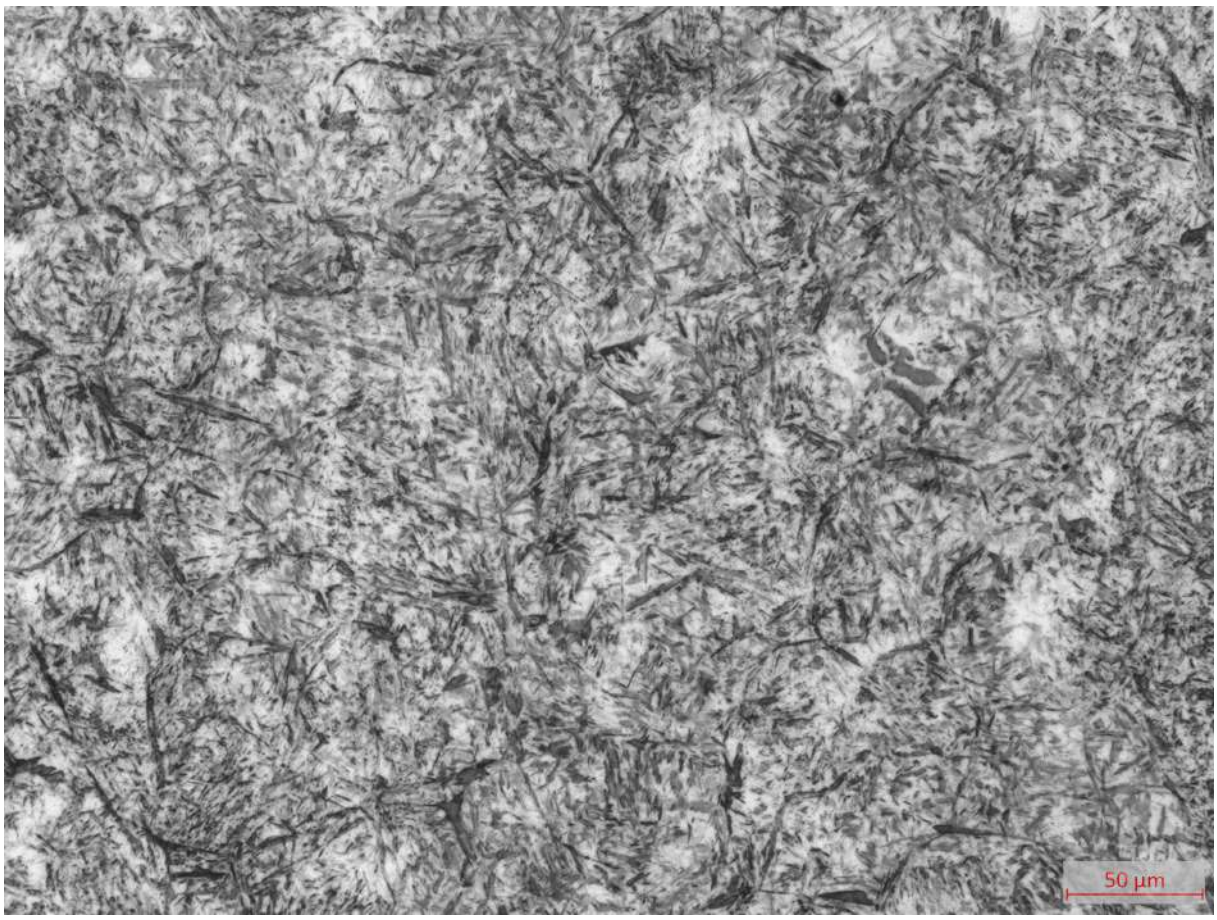


**Figure B.5:** *Q, 500x magnification*

## B.2 200x

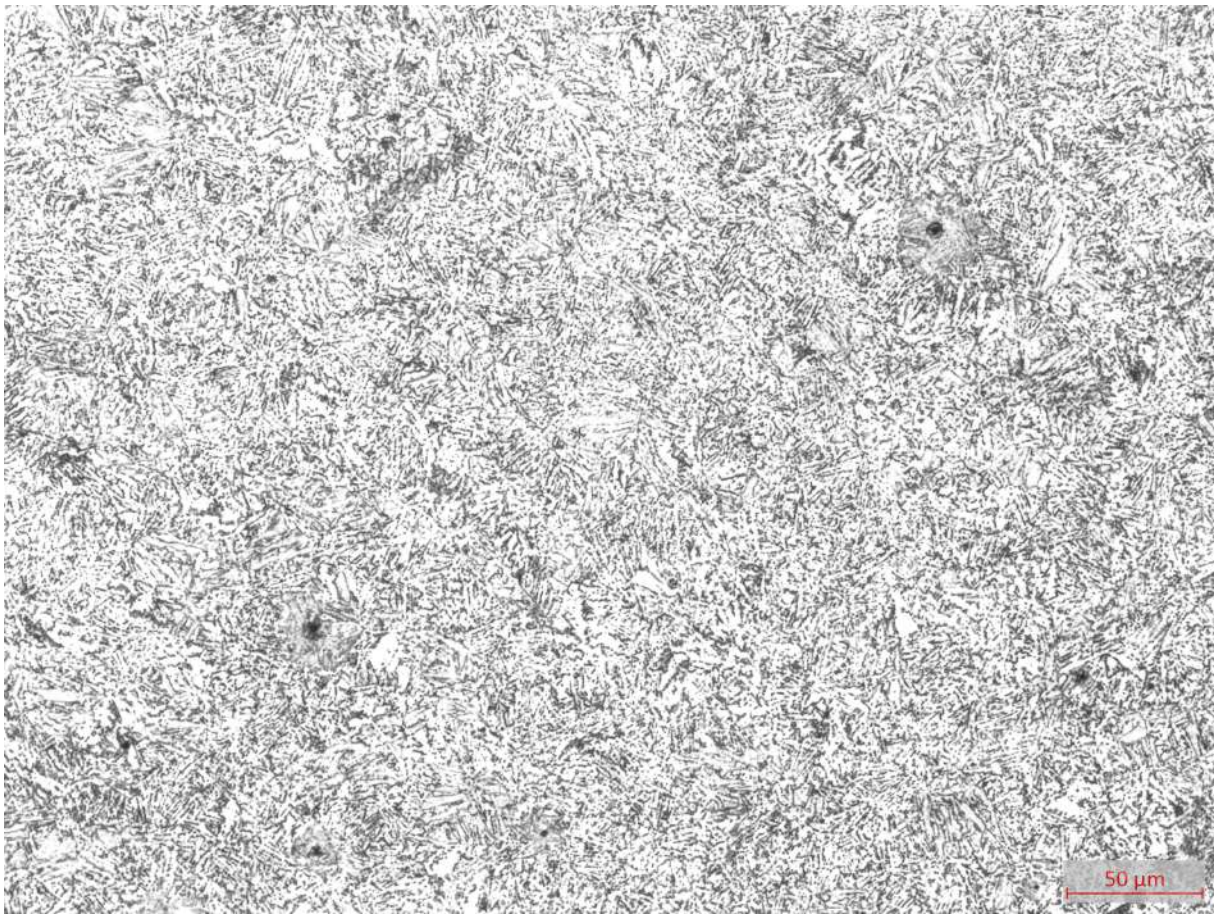


**Figure B.6:** *D, 200x magnification*

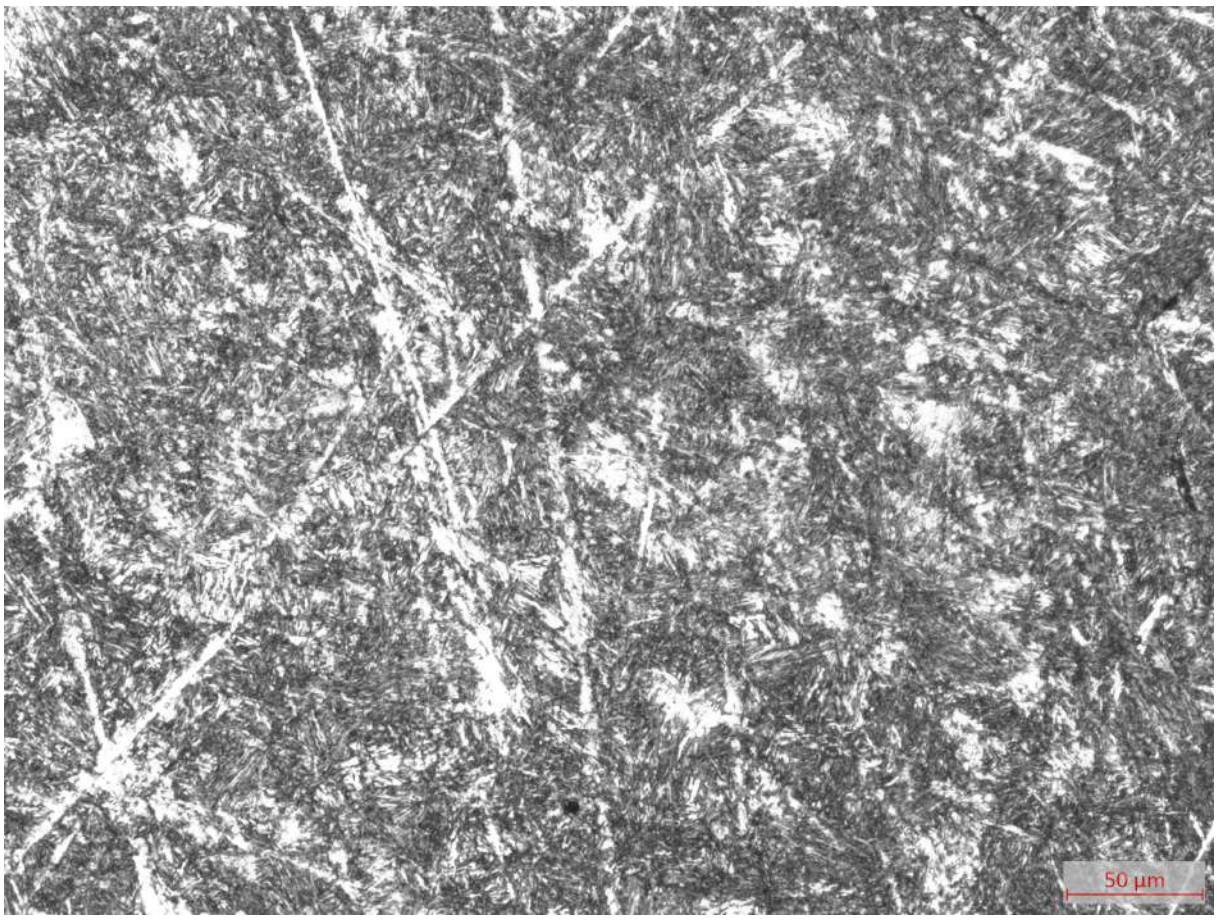


**Figure B.7:** *B240, 200x magnification*

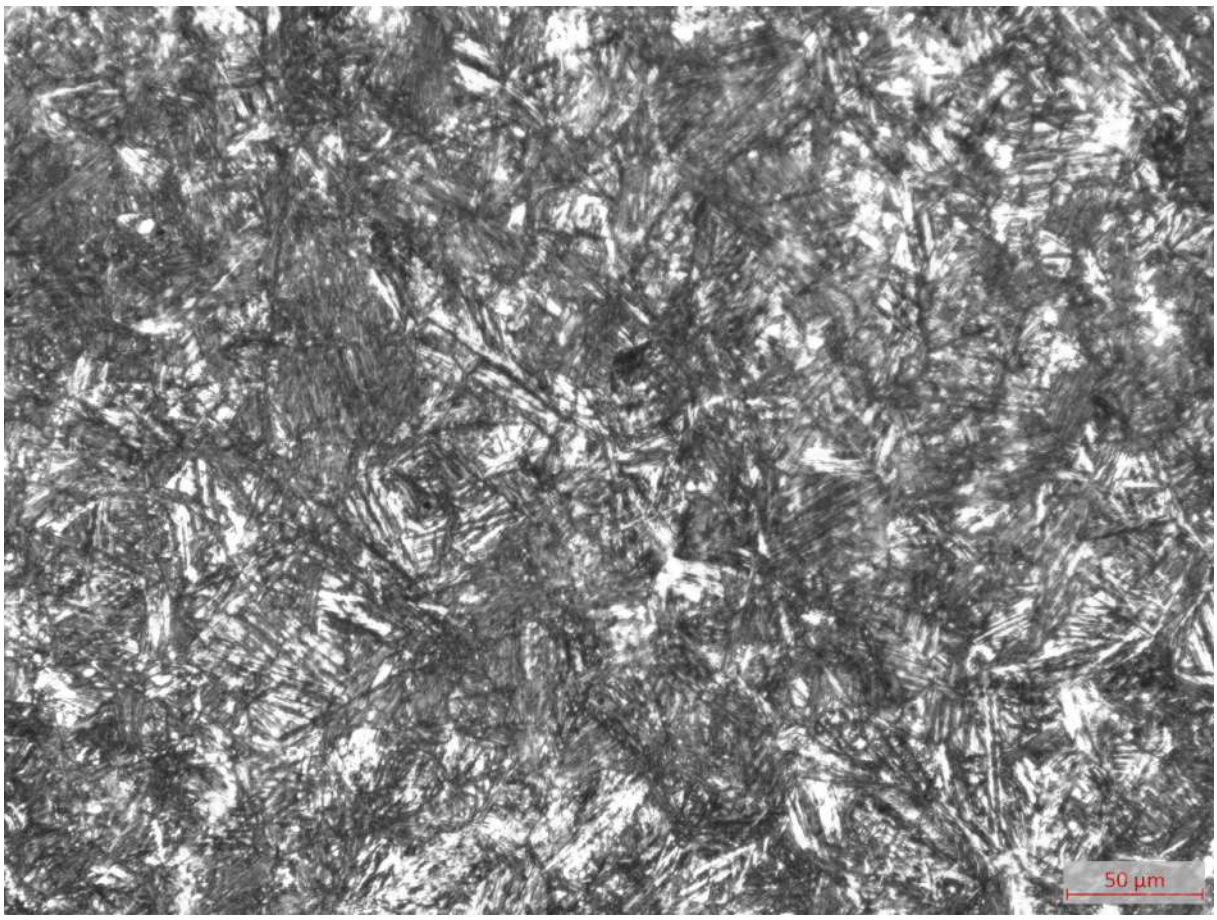


**Figure B.8:** *B280, 200x magnification*

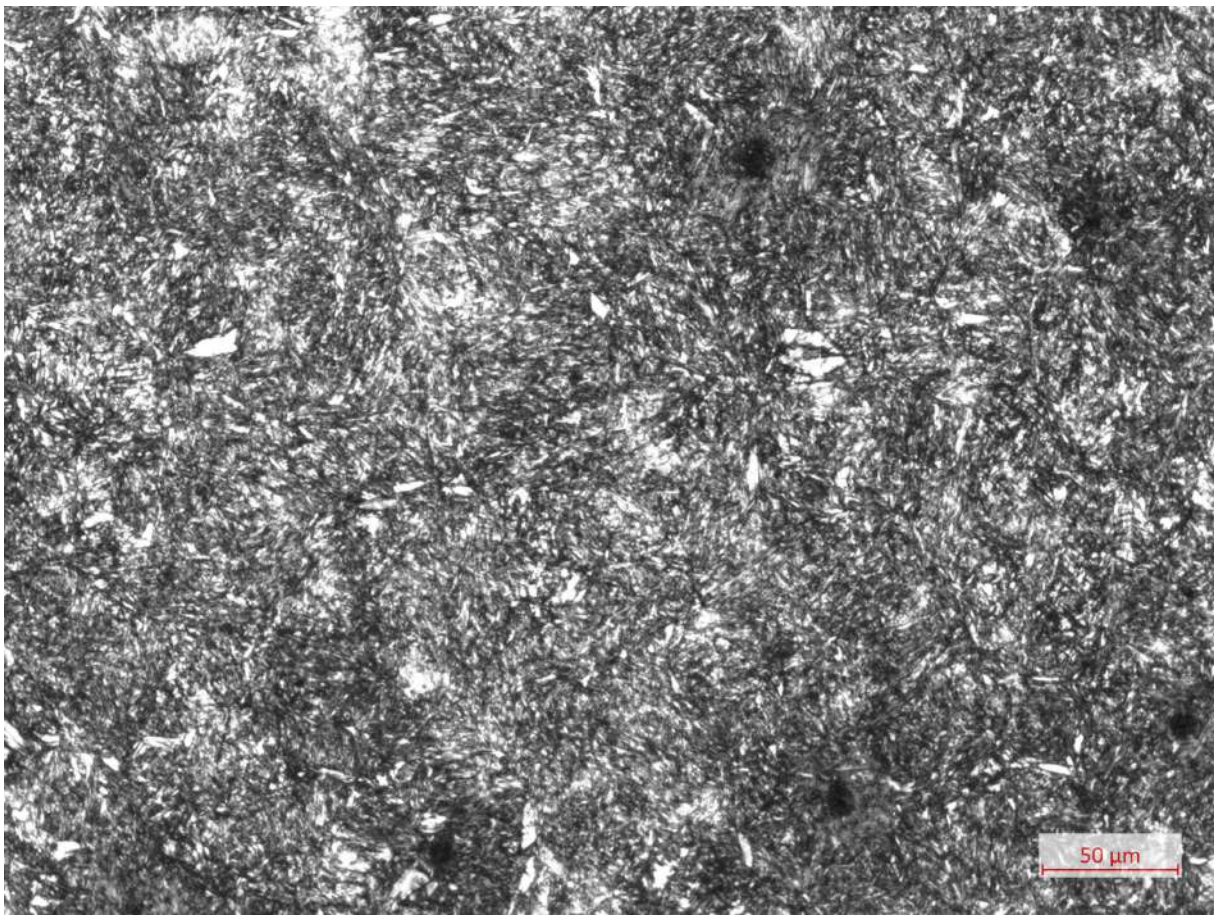


**Figure B.9:** *QT440, 200x magnification*

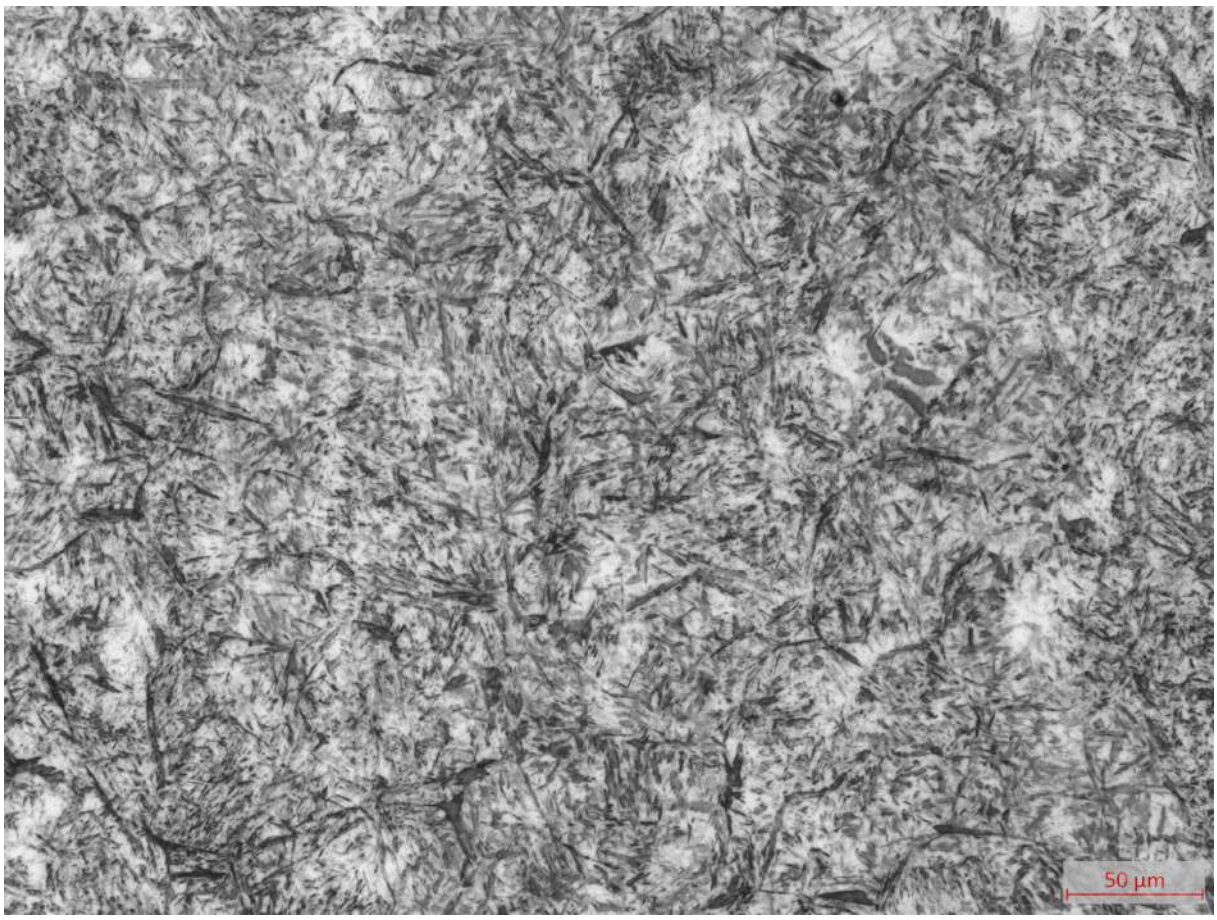


**Figure B.10:** *Q, 200x magnification*

## B.3 100x

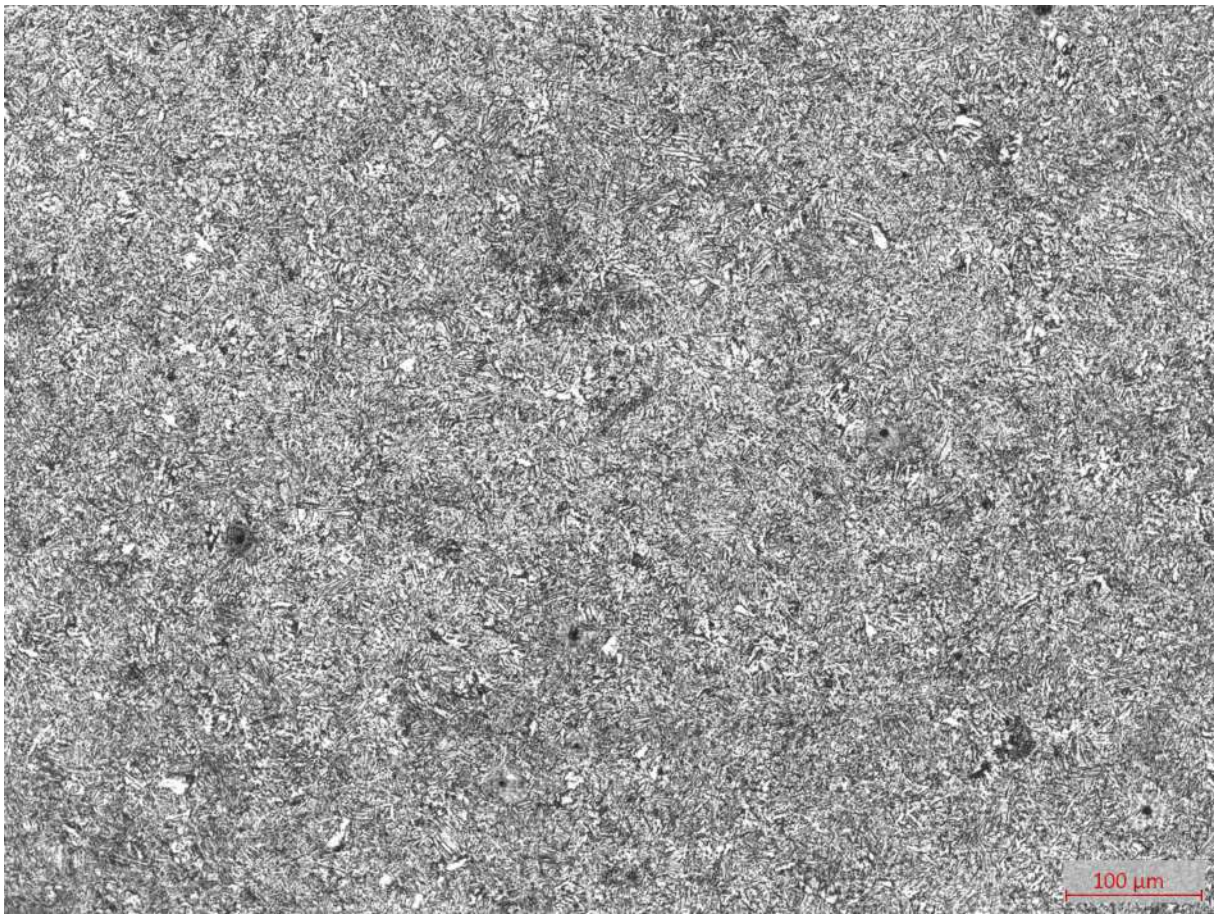


**Figure B.11:** *D, 100x magnification*

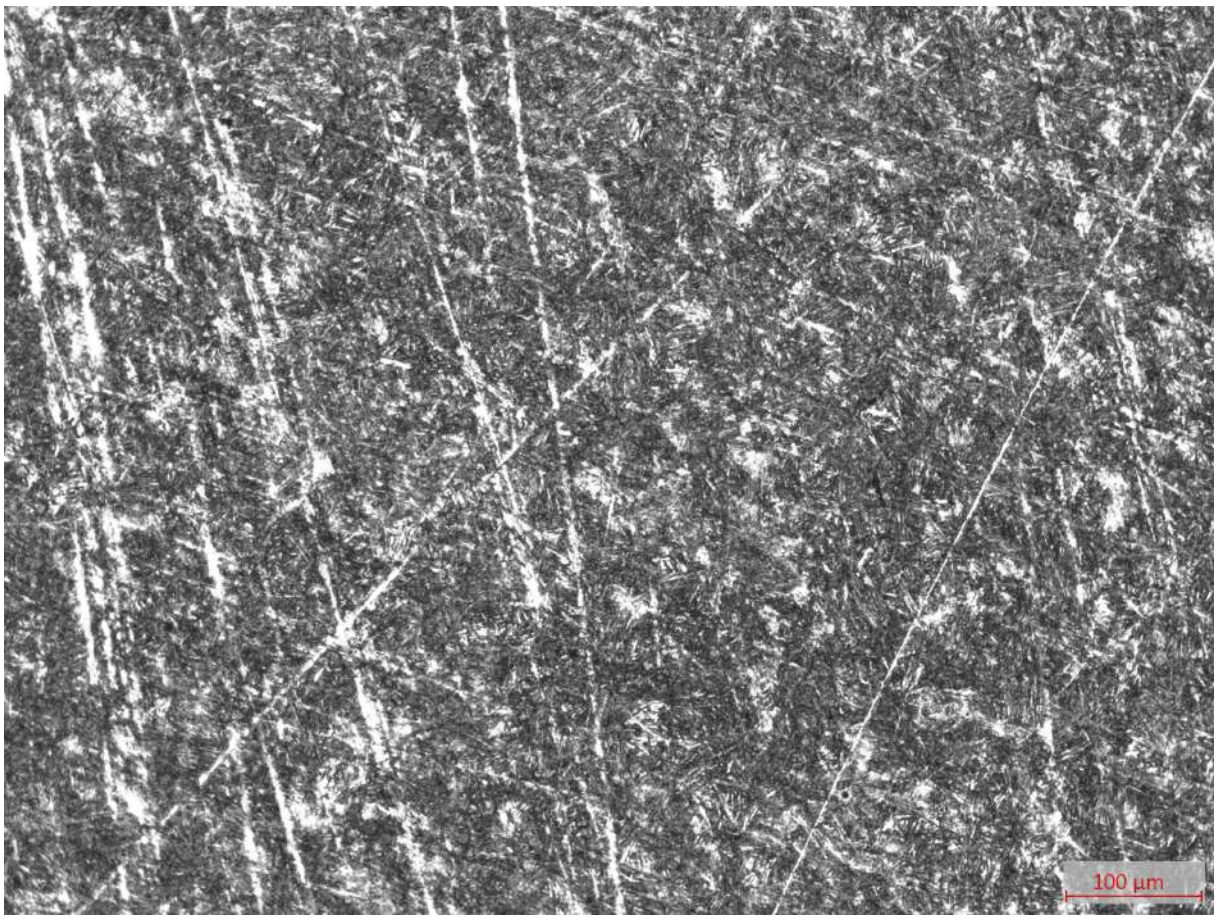


**Figure B.12:** *B240, 100x magnification*

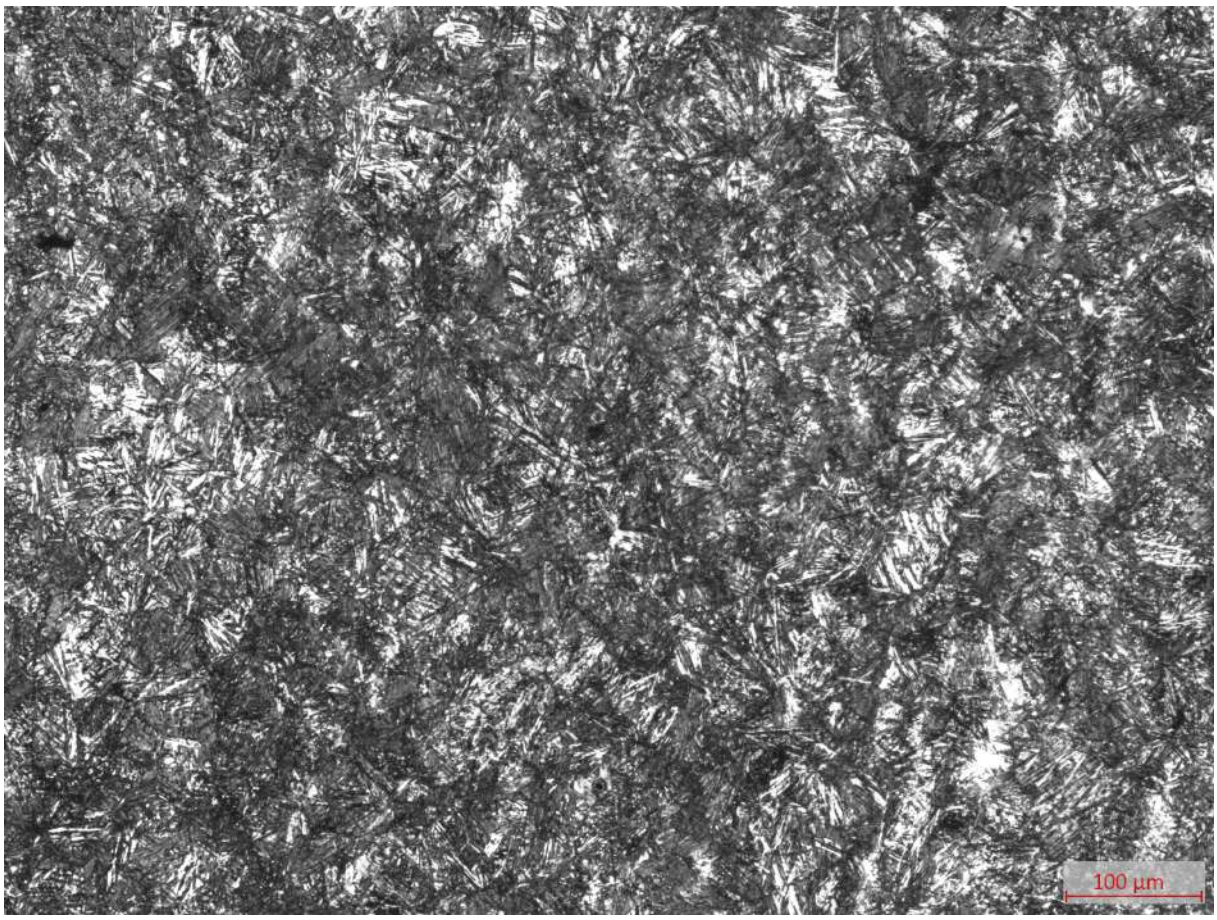


**Figure B.13:** *B280, 100x magnification*

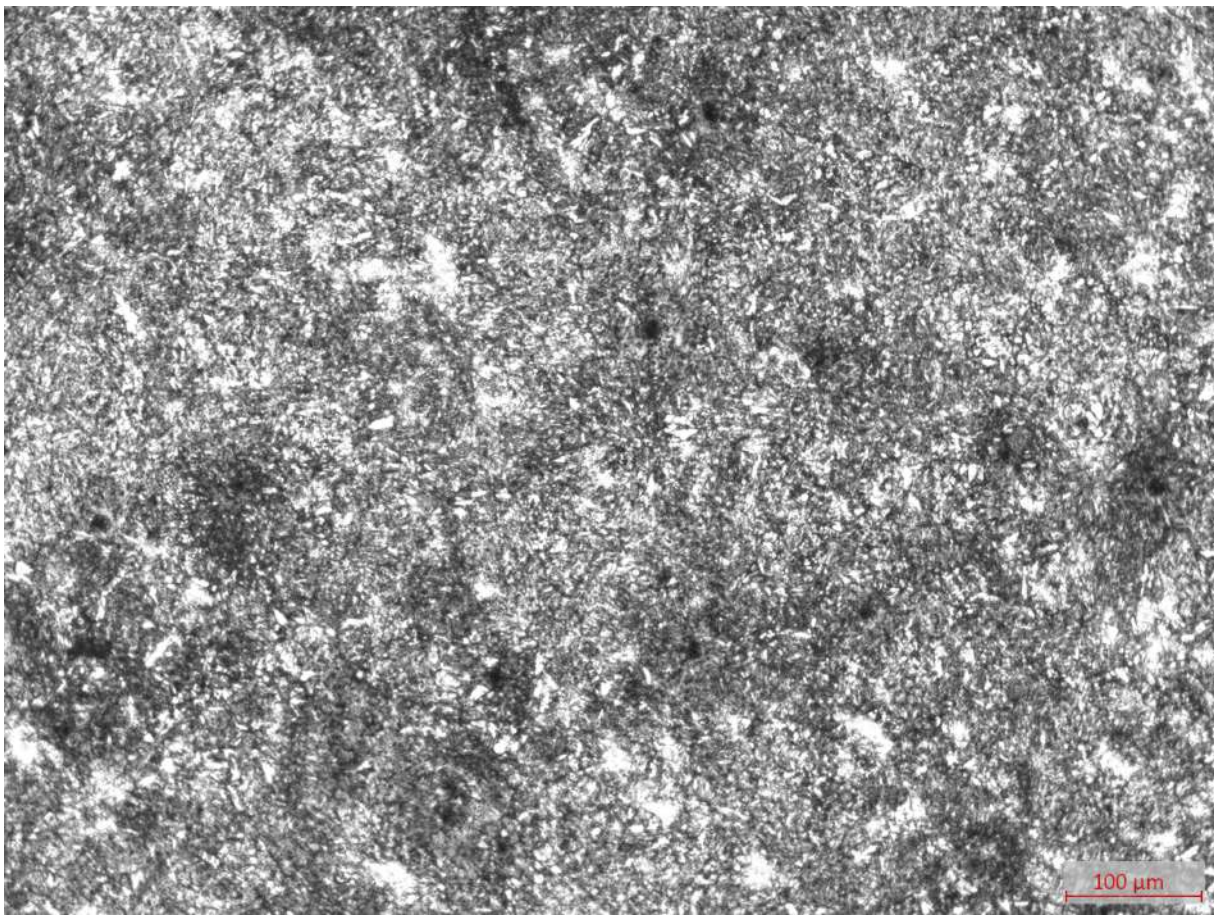


**Figure B.14:** *QT440, 100x magnification*

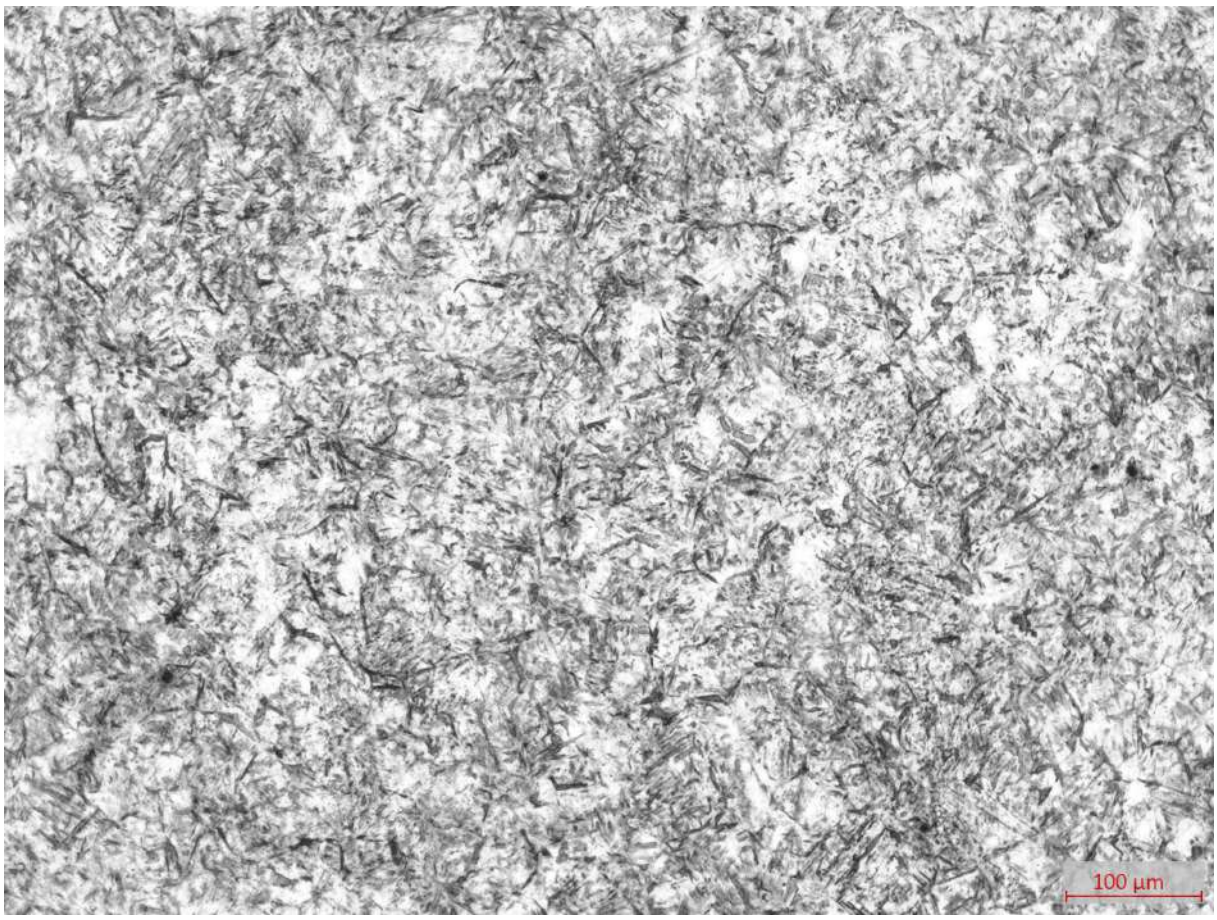


**Figure B.15:** *Q, 100x magnification*

## B.4 50x

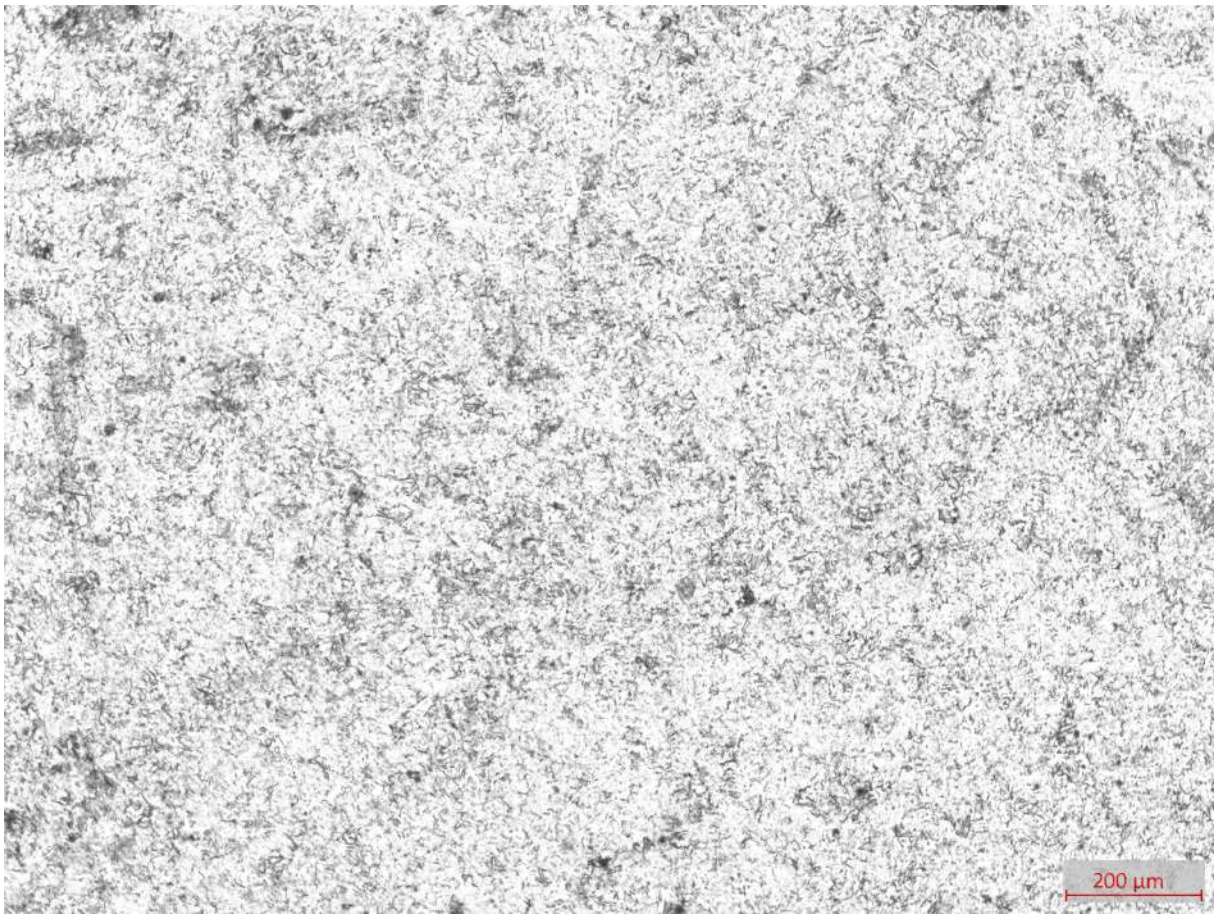


**Figure B.16:** *D, 50x magnification*

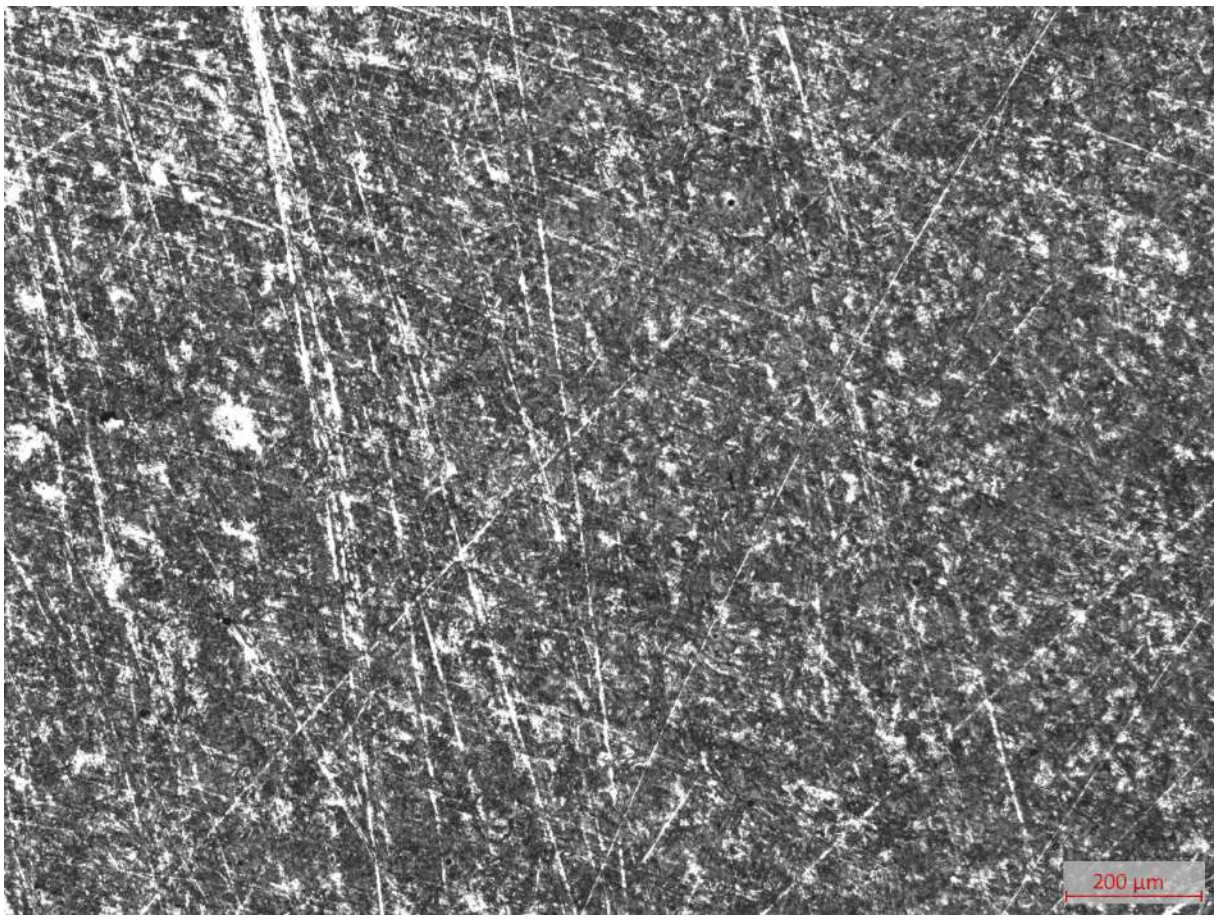


**Figure B.17:** *B240, 50x magnification*

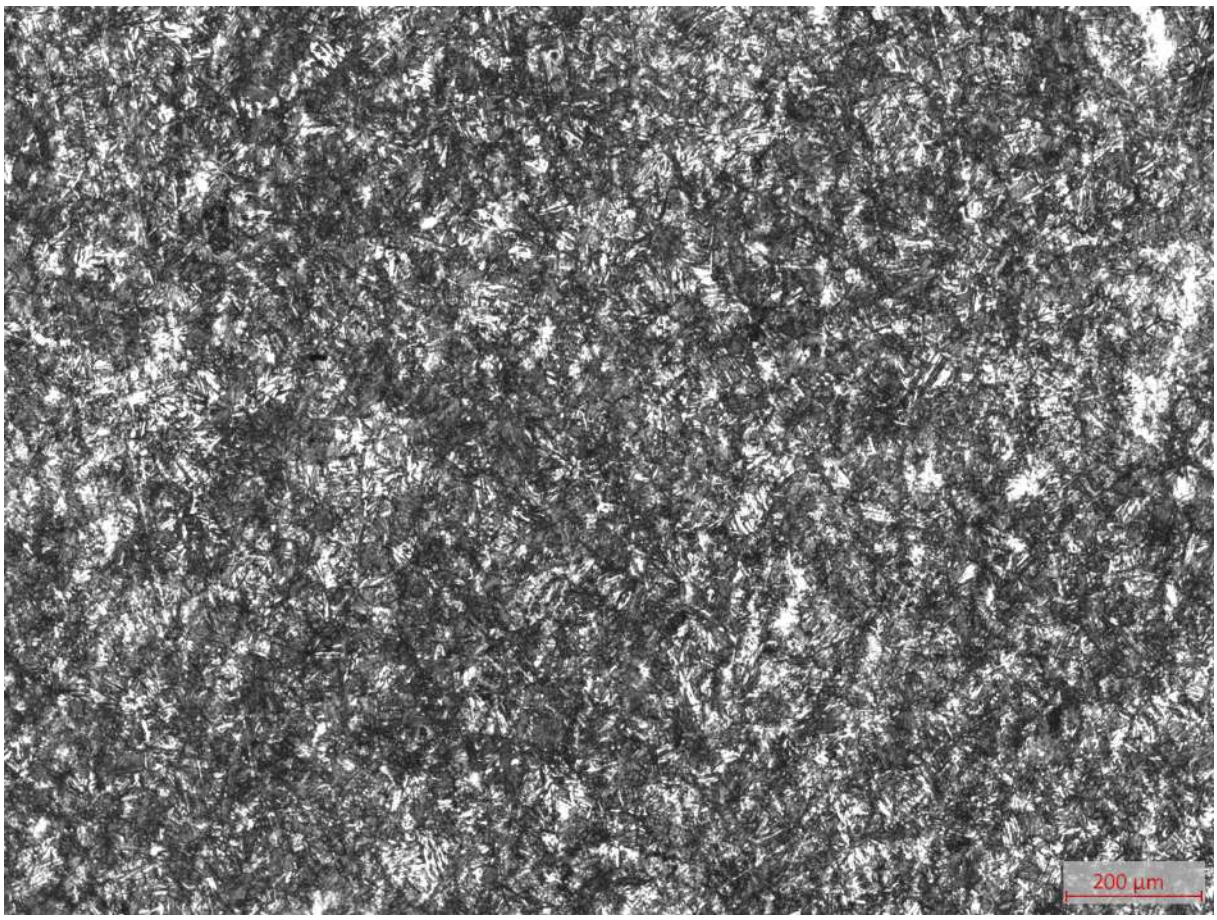


**Figure B.18:** *B280, 50x magnification*

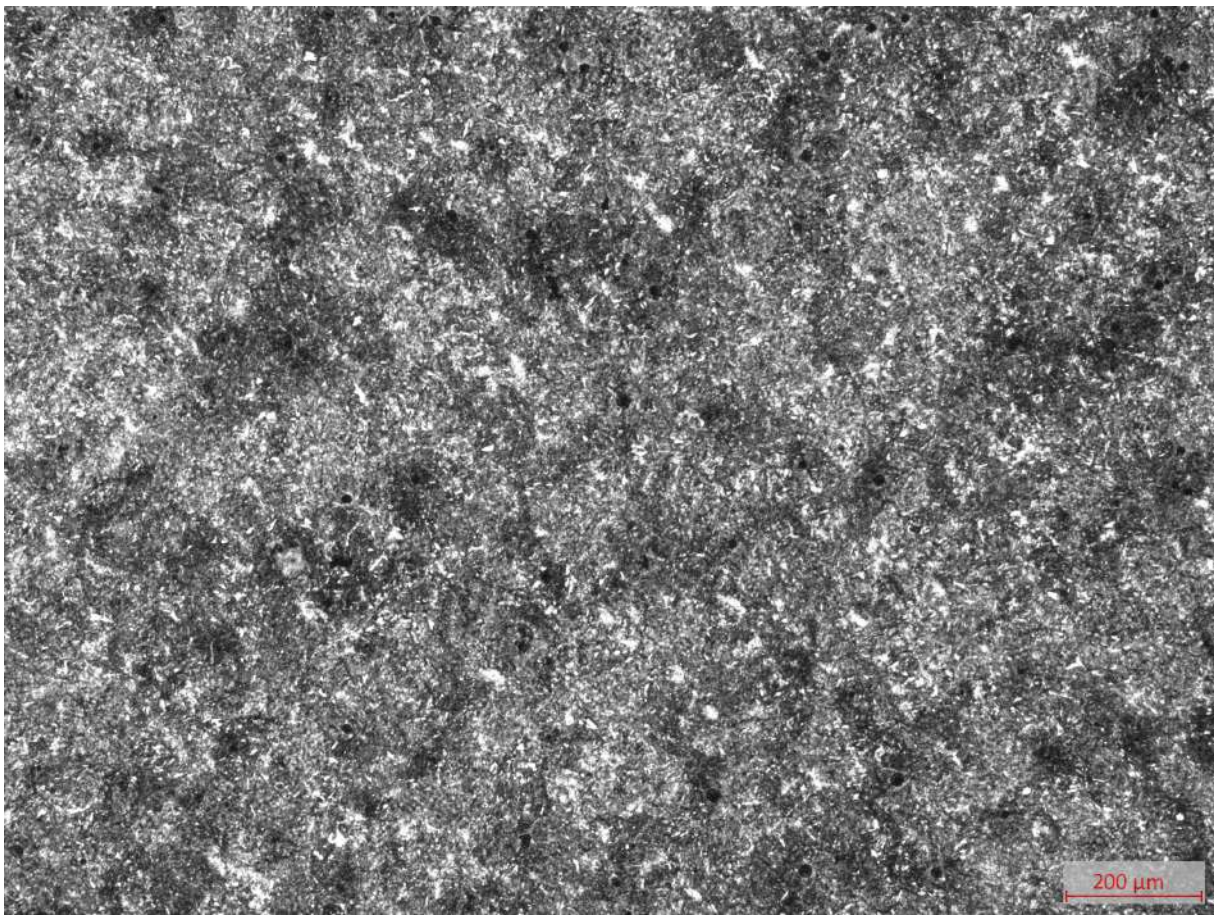


**Figure B.19:** *QT440, 50x magnification*

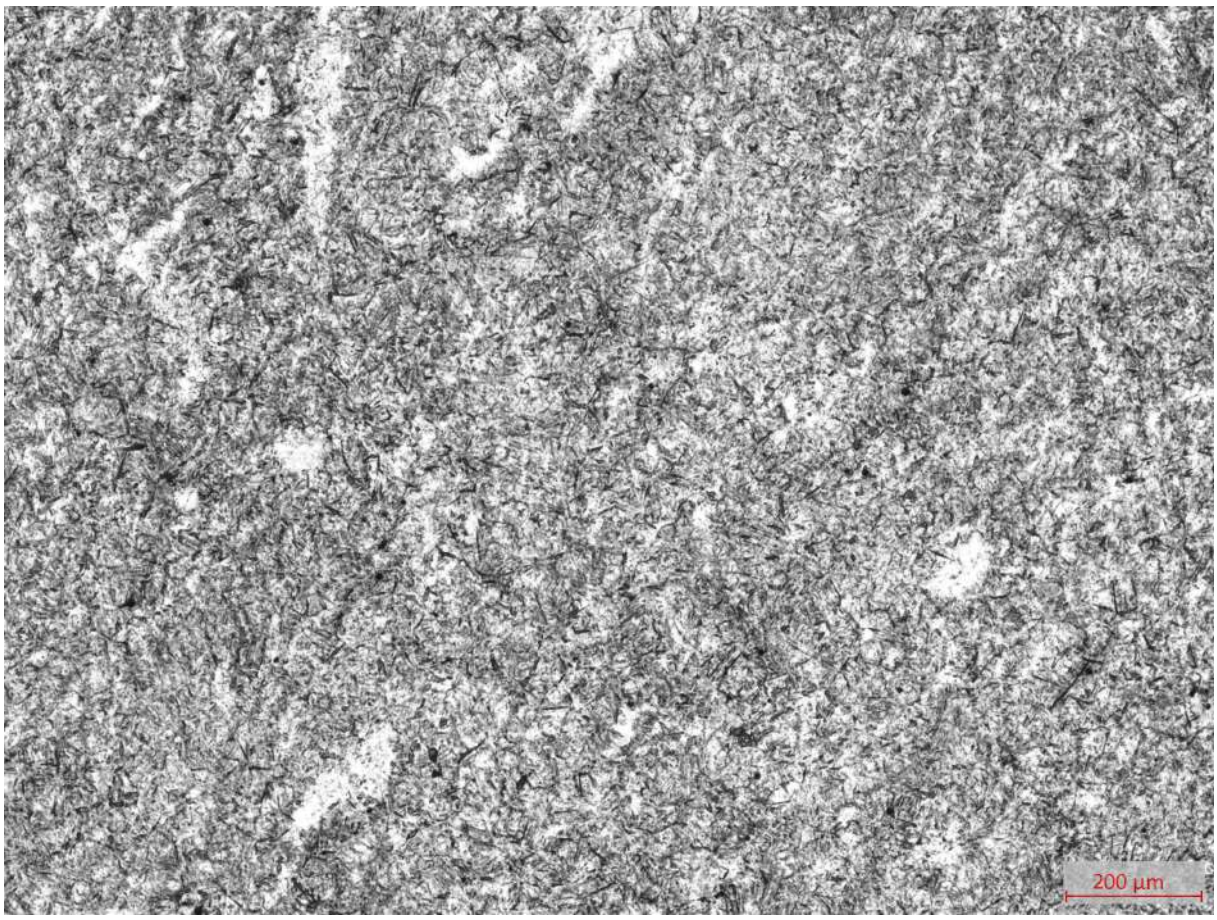


**Figure B.20:** *Q, 50x magnification*